New insights on the ^{7}Be cycle in the ocean

Mélanie Grenier, Pieter van Beek, Paul Lerner, Virginie Sanial, Marc Souhaut, Marion Lagarde, Olivier Marchal, Jean-Louis Reyss

New insights on the ^{7}Be cycle in the ocean

Grenier M.[1,*], van Beek P.[1], Lerner P.[2,3], Sanial V.[4], Souhaut M.[1], Lagarde M. [1], Marchal O.[5], Reyss J.L. [6]

[1] LEGOS, University of Toulouse, CNRS, CNES, IRD, UPS, Toulouse, 31400, France

[2] NASA-GISS, New York City, NY, 10025, USA

[3] Department of Applied Physics and Applied Mathematics, Columbia University, New York City, NY, 10027, USA

[4] Université de Toulon, Aix Marseille Univ., CNRS, IRD, MIO, Toulon, 83041, France

[5] Woods Hole Oceanographic Institution, Woods Hole, MA, 02543, USA

[6] Laboratoire des Sciences du Climat et de l'Environnement, Gif-sur-Yvette, 91198, France

* Corresponding author: Mélanie Grenier (melanie.grenier@legos.obs-mip.fr)

Abstract

The cosmogenic radionuclide ^{7}Be has been applied as a tracer of dynamical processes in the upper ocean and of atmospheric deposition of trace elements at the sea surface. These applications usually assume that ^{7}Be is entirely in the dissolved form, and that scavenging and downward export of ^{7}Be by settling particles can be neglected. In this work, we explore these assumptions and more generally assess the significance of the ^{7}Be activity in the particulate fraction, through the generation of vertical profiles of particulate ^{7}Be in the open ocean. From detailed measurements obtained from low-background gamma spectrometers placed in underground facilities, we report vertical profiles of ^{7}Be activity in suspended particles ($^{7}Be_{p}$) collected in various oceanic regions: the Mediterranean Sea (DYFAMED station), the Indian Sector of the Southern Ocean (station A3-2 from the KEOPS2 cruise), the Sargasso Sea (OFP station), and the subpolar North Atlantic Ocean (GEOVIDE cruise).

We find that, in each oceanic region, $^{7}Be_{p}$ activities are generally higher in the mixed layer than in the thermocline. They vary in the mixed layer from 3.0 dpm/m^{3} at DYFAMED to 33.1dpm/m^{3} at GEOVIDE cross-over station 51/60, i.e., within a range consistent with previous $^{7}Be_{p}$ measurements for the open ocean. For the GEOVIDE cruise, the $^{7}Be_{p}$ activities measured on different filter types at different depths are corrected for filter offsets derived from multiple $^{7}Be_{p}$ measurements at a near-coastal station in the western Mediterranean Sea. We then combine measurements of total ^{7}Be activity (Shelley et al., 2017) with our measurements of $^{7}Be_{p}$ activity to estimate the solid/solution partitioning of ^{7}Be. On average, the particulate fraction would represent 6% of total ^{7}Be activity at 5-m water depth (n = 6), 22% at 20 m (n = 2) and 9% at 70

m (n = 3). At GEOVIDE stations, $^{7}Be_{p}$ inventories range from 5% to 19% of the total ^{7}Be inventories. In the Labrador Sea, the measured $^{7}Be_{p}$ inventories are lower than the dry ^{7}Be deposition fluxes estimated from aerosol samples collected during GEOVIDE, suggesting that a significant portion of $^{7}Be_{p}$ may be removed by sinking particles. The distribution coefficient K_d for ^{7}Be increases with depth, with $\log_{10}K_d$ averaging 5.2 ± 0.1 at 5 m to 6.1 ± 0.1 between 70 and 150 m, suggesting that scavenging of dissolved ^{7}Be by particles is more pronounced in the thermocline than in the mixed layer when differences in particle concentrations are taken into account. Overall, our study suggests that, at least in some oceanic regions, the removal of ^{7}Be by marine particles may be significant and that it may need to be considered in applications of ^{7}Be as a tracer of oceanic processes and atmospheric deposition.

Keywords: Beryllium-7; suspended particles; vertical profiles; open ocean; solid/solution partitioning; GEOTRACES

1. Introduction

Beryllium-7 (^{7}Be) is produced in the atmosphere by cosmic ray spallation mostly of oxygen and nitrogen nuclei (Lal and Peters, 1967). ^{7}Be then enters the marine and terrestrial environments via wet and dry depositions (Feely et al., 1989). The relatively short half-life of ^{7}Be (53.3 days; Browne et al., 1978) makes it a useful tracer of processes in the coastal ocean and the open upper ocean on seasonal and regional time-scales.

In estuaries and coastal environments, ^{7}Be can be quickly scavenged by particles (Aaboe et al., 1981; Dibb and Rice, 1989; Olsen et al., 1986). Several studies have reported a significant affinity of ^{7}Be for particles in these environments, where the distribution coefficients K_d for ^{7}Be can be of the order of 10^5 cm^3/g, with K_d being the ratio of particulate ^{7}Be activity to dissolved ^{7}Be activity, normalized to particle concentration (Baskaran and Santschi, 1993; Dibb and Rice, 1989). Consistent with this result, ^{7}Be has been applied in coastal and estuarine systems to study short-term variations of sediment accumulation rate and sediment transport (e.g., Dibb and Rice, 1989; Wu et al., 2018).

In the open ocean, ^{7}Be is generally well mixed in the surface mixed layer, and decreases about exponentially with depth in the upper thermocline (Aaboe et al., 1981; Kadko et al., 2015; Kadko and Olson, 1996; Silker, 1972a; Young and Silker, 1980). This pattern has led to the use of ^{7}Be for quantifying mixing in the thermocline and surface water subduction (e.g., Kadko and Olson, 1996), as well as upwelling rates (Haskell et al., 2015; Kadko, 2017; Kadko and Johns, 2011). Recently, Kadko et al. (2015) used the inventory of ^{7}Be measured in the upper water

column to estimate the atmospheric deposition fluxes of other trace elements in remote oceanic regions (Kadko et al., 2019; Shelley et al., 2017).

Many of these applications of ^{7}Be as a tracer of oceanic and atmospheric processes rely on the assumption that ^{7}Be behaves conservatively in seawater, i.e., that radioactive decay is the only sink for ^{7}Be. Previous studies on ^{7}Be cycling in the open ocean usually considered that ^{7}Be occurs predominantly in the dissolved form and neglected particulate scavenging (adsorption of dissolved ^{7}Be onto particles) and downward export by settling particles. These assumptions are based on evidence that ^{7}Be is relatively soluble in low particle environments such as in the oligotrophic regions of the open ocean (Aaboe et al., 1981; Kadko and Prospero, 2011). However, particulate ^{7}Be ($^{7}Be_{p}$) measurements are scarce in the open ocean. ^{7}Be activity in suspended particles has been rarely determined, and the few particulate ^{7}Be measurements that are available are found mostly in the mixed layer (Andrews et al., 2008; Kadko and Johns, 2011; Kremenchutskii et al., 2021; Silker, 1972b, 1972a; Silker et al., 1968). For example, Andrews et al. (2008) reported ^{7}Be activities below the detection limit in a particulate sample collected by pumping 1000 L of surface water in the Sargasso Sea. From a study conducted in the upper 100 m of the Sargasso Sea off Bermuda, Silker (1972a) concluded that < 10% of the ^{7}Be was present in the particulate form. However, to our knowledge, no $^{7}Be_{p}$ measurements exist below a water depth of 100 m.

Regarding the atmospheric ^{7}Be source, it is often considered that ^{7}Be enters the surface ocean primarily via precipitation (wet deposition), although our understanding of ^{7}Be deposition in terrestrial and marine environments remains limited. For instance, Gaffney et al. (1994) analysed rain samples from Illinois and New Mexico (USA), and concluded that ^{7}Be was primarily in the dissolved form, the particulate ^{7}Be representing only 1.2 to 12.1% of total (dissolved + particulate) ^{7}Be. On the other hand, Papastefanou and Ioannidou (1996) analyzed aerosols sampled near Thessaloniki (Greece), and reported that particulate ^{7}Be (nominal filter pore size = 1.1 μm) could represent 20-50% of the total ^{7}Be activity in aerosols. The wet and dry depositions of ^{7}Be to the surface ocean are even less well constrained.

Similarly, the significance and fate of particulate ^{7}Be deposited at the sea surface have been rarely investigated. Dissolution of aerosols in the ocean mixed layer may release into solution ^{7}Be present at the surface and/or within the aerosol particles. Alternatively, adsorption of dissolved ^{7}Be onto settling particles may remove a significant fraction of ^{7}Be from solution. Aggregation of small particles to form larger particles may further increase the vertical flux of particulate ^{7}Be to deep waters by increasing particle settling speeds (e.g., Burd and Jackson,

2009). The removal of ^{7}Be from the surface ocean by attachment to settling particles may impact the vertical distribution of dissolved ^{7}Be and may thus introduce biases in ^{7}Be-based estimates of dynamical parameters such as vertical eddy diffusivity (e.g., Haskell, Kadko, et al., 2015; Kadko and Olson, 1996) and upwelling rate (e.g., Kadko and Johns, 2011).

Similarly, the method developed by Kadko et al. (2015) to estimate trace element (TE) atmospheric fluxes could suffer from a bias, should particle scavenging and export, in addition to radioactive decay, be a significant sink of ^{7}Be. In order to assess whether scavenging and export of ^{7}Be by settling particles can be neglected in the open ocean, the significance of particulate ^{7}Be and the exchange of ^{7}Be between the dissolved and particulate phases need to be better constrained.

Here we report measurements of ^{7}Be activity determined in suspended particles collected between 2002 and 2014 in the upper water column in different oceanic regions. Through paired estimates of ^{7}Be activity in the particulate and total phases, our goals are (i) to provide constraints on the solid-solution partitioning of ^{7}Be in different oceanic environments, (ii) to develop a better understanding of the processes affecting the cycling of this cosmogenic isotope in the water column, and (iii) to assess the applicability of ^{7}Be as a tracer of transport processes in the ocean and of the deposition of TEs at the sea surface.

2. Methods

2.1 Sampling

^{7}Be activities were determined in suspended particle samples collected at different depths in four different oceanic regions (Tables 1 and 2; Figure 1): 1) at the OFP (Oceanic Flux Program) station off Bermuda in the Sargasso Sea in May 2002, aboard the R/V *Weatherbird II* (PIs: Maureen Conte and Roger François; van Beek et al., 2007); 2) at the DYFAMED (Dynamics of Atmospheric Fluxes in the MEDiterranean sea) station in the western Mediterranean Sea in March and May 2003 during the BARMED project, aboard the R/V *Téthys II* (PI: Catherine Jeandel; van Beek et al., 2009); 3) at station A3-2 on the Kerguelen Plateau in the Southern Ocean in November 2011 during the KEOPS2 project, aboard the R/V *Marion Dufresne* (PI: Stéphane Blain); and 4) at nine stations of the GEOVIDE section completed in the North Atlantic in May-June 2014, aboard the R/V *Pourquoi Pas?* (GEOTRACES cruise GA01; PIs: Géraldine Sarthou and Pascale Lherminier). The suspended

particles were collected using different types of filters with 0.8-1 µm nominal porosity and 142-mm diameter mounted on McLane large volume pumps. After collection, the filters were stored at room temperature in petri dishes until their return to the laboratory. Specifically, 0.8-µm pore size Versapor filters were used for OFP and BARMED cruises, and 0.8-µm pore size Supor filters were used for KEOPS2. For the GEOVIDE cruise, we used either 1 µm-pore size QMA filters or 0.8-µm pore size Supor filters. During GEOVIDE, surface samples (ca. 5 m below the sea surface) were also collected using the ship seawater intake and were filtered through pocket filters (polypropylene filters Pentek BP-410-1; hereafter referred as socks) with a pore size of 1 µm. This method allows the filtration of very large volumes of seawater, although it is not a conventional technique for collecting particulate samples for TE analyses. Filters such as Versapor, QMA, and Supor are more commonly used to collect suspended particles in marine environments.

The use of different filter types may generate systematic differences in the measured $^{7}Be_{p}$ activities, as was observed for $^{234}Th_{p}$ measured on different quartz filters (glass fiber filters, or GF/F, and microquartz filters; Benitez-Nelson et al., 2001; Maiti et al., 2012). In particular, $^{7}Be_{p}$ measurements at different depths are combined in this study to generate vertical profiles of $^{7}Be_{p}$ at GEOVIDE stations, although at these stations ^{7}Be activities at different depths have been measured on different filter types. In Section 4.2, we assess the impact of the different filter types used for GEOVIDE on the determination of $^{7}Be_{p}$ activity, and we derive filter-specific corrections for the GEOVIDE $^{7}Be_{p}$ activities.

During GEOVIDE, total ^{7}Be activities (i.e., sum of dissolved and particulate ^{7}Be activities) were also determined on unfiltered samples gathered at different depths at the same stations as those considered in this study (Shelley et al., 2017). However, samples dedicated to particulate and total ^{7}Be analyses came from different casts, and some of these casts exhibited significant differences in vertical density profiles (sections 4 and 5). As a result, some caution should be exercised when combining the measurements of total and particulate ^{7}Be at GEOVIDE stations.

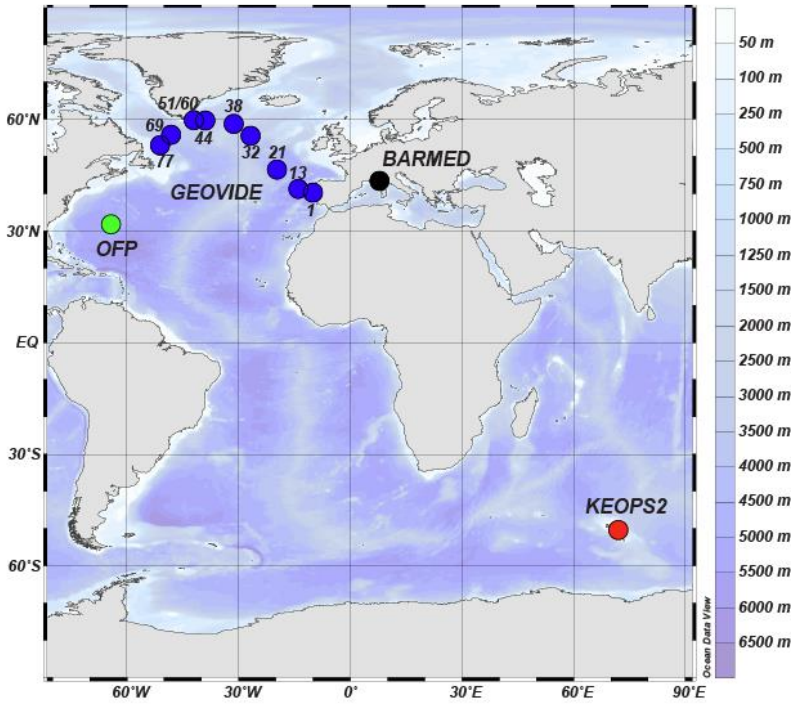

Figure 1: Stations where samples for ^{7}Be measurements were collected and analysed in this study. These samples were collected in the framework of different programs: OFP in the Sargasso Sea (green dot), BARMED in the Mediterranean Sea (black dot), KEOPS2 in the Southern Ocean (red dot), and GEOVIDE/GA01 in the North Atlantic (blue dots).

2.2 ^{7}Be analyses

Upon return to the laboratory, the particulate (filter) samples were folded and sealed in counting tubes. The analyses of $^{7}Be_{p}$ were conducted within two weeks to four months of the arrival of the samples in the laboratory, using low background gamma-ray spectrometers at two different facilities: the laboratory LAFARA (Laboratoire de mesure des Faibles Radioactivités; Université Toulouse III Paul Sabatier; van Beek et al., 2013) in the French Pyrénées, and the laboratory of Modane in the French Alps (Reyss et al., 1995). Both laboratories host high-purity germanium (HPGe) gamma-ray spectrometers manufactured with selected materials. Both are underground, so that the detectors are protected from the influence of cosmic rays and provide very low background levels (Reyss et al., 1995; van Beek et al., 2013). The filter samples were placed within the germanium crystals (well-type detectors), which allowed us to further increase the sensitivity of the analyses. By combining the low background levels achieved at LAFARA and Modane with the use of sensitive well-type detectors, very low levels of radioactivity could be quantified. The ^{7}Be activities were determined using the 477.6 keV gamma line. Due to the lack of any reference material for ^{7}Be, we determined the efficiency at 477.6 keV from the efficiency curve obtained from different reference materials (RGU-1,

RGTH-1 and #375) provided by the International Atomic Energy Agency (Martínez-Ruiz et al., 2007).

The uncertainties of the $^{7}Be_{p}$ activities measured at LAFARA and Modane and reported in this study are 1 sigma uncertainties (counting statistics). The relative uncertainties range from 3% to 33% for samples collected in the upper 300 m (14% on average) and can be higher for samples collected below 300 m. Note that the precision on the ^{7}Be activity primarily depends on the number of counts determined by the gamma spectrometers, which itself depends on different parameters, including i) counting time, ii) sample volume (larger volumes may lead to higher count rates), iii) the time elapsed between sampling and analysis (a short time will limit loss of ^{7}Be by radioactive decay), and iv) the sensitivity of the gamma spectrometers (the large, well-type detectors that are placed underground and that are used for this study tend to reduce the background). The detection limits for ^{7}Be are 0.36-0.48 dpm for the well-type detectors at LAFARA. The detection limits were not determined for the gamma spectrometers at Modane, but they can reasonably be assumed similar or even slightly lower.

LAFARA regularly participates to interlaboratory comparison exercises organized by the French institution IRSN (Institut de Radioprotection et Sûreté Nucléaire) to evaluate the ability of this laboratory to quantify natural and artificial radionuclides in various substrates. The accuracy of radionuclide measurements at LAFARA is thus regularly tested. Because LAFARA successfully participated to these exercises and follows the recommendations of the international standard ISO/CEI-17025, this laboratory has been certified by the French Nuclear Safety Authority (Autorité de Sûreté Nucléaire, ASN). Although ^{7}Be is not part of the interlaboratory comparison organized by IRSN, overall, the successful analysis of gamma emitters with a wide range of energies (30-2500 keV) validates the efficiency curves of the gamma spectrometers (calibration of the detectors), which are key for the quantification of accurate radionuclide activities.

LAFARA also participated to an interlaboratory comparison exercise organized by the GEOTRACES Standards and Intercalibration Committee to evaluate the ability to quantify ^{7}Be activity in water samples. This exercise involved six laboratories worldwide and aimed at testing accuracy, precision, and reproducibility by preparing and analysing three replicates (W. Geibert, unpublished data). Overall, the different labs involved reported ^{7}Be activities that are in good agreement with each other. The mean ^{7}Be activity of the three replicates analysed by LAFARA was 162.6 ± 4.8 dpm/kg (3% precision with the 1 sigma uncertainty). The mean of

162.6 dpm/kg was within the one standard deviation of the mean ^{7}Be activity measured by the six labs (149.4 ± 14.4 dpm/kg). Note that, at the different stations reported here, we did not analyse replicates because the large seawater volumes needed to quantify ^{7}Be usually prevent from collecting replicates.

2.3 Suspended particle matter (SPM) concentration

Concentrations of suspended particle matter ([SPM]) were estimated following the method described in Lam et al. (2015) from the concentrations of particulate lithogenic matter, organic matter, opal, calcium carbonate, iron (Fe) hydroxides, and manganese (Mn) oxides. Particulate organic matter concentration was determined from concentrations of particulate organic carbon and biogenic silica (Sarthou et al., 2018). Lithogenic matter concentration was determined from concentrations of particulate aluminum, calcium carbonate from particulate calcium, Fe hydroxides from particulate Fe, and Mn oxides from particulate Mn (Gourain et al., 2019). These analyses were not performed on the filters dedicated to ^{7}Be analysis but on (i) filters dedicated to lead-210 and polonium-210 analyses (^{210}Pb-$^{-210}$Po) mounted on *in situ* pumps (ISP; Y. Tang et al., 2018) and on (ii) filter samples collected from Niskin and Go-Flo bottles, as described in Lagarde et al. (submitted). We generally used [SPM] estimates determined from bottle samples rather than those determined from ISP samples (Tang et al., 2018); the rosette samples have greater vertical resolution than the ISP samples, especially in the upper 40 m of the water column, which provides a better agreement with the depths of $^{7}Be_{p}$ samples. The [SPM] estimated from Niskin/Go-Flo and ISP samples are compared in section 5.4.

3. Oceanographic context

We chose to measure particulate ^{7}Be on samples collected at OFP (Sargasso Sea) and DYFAMED (Mediterranean Sea), since oceanographic conditions at these stations are relatively well documented, particularly through time series programs. The OFP sediment trap time series mooring (Conte et al., 2001) is located in the northern Sargasso Sea (4,200 m water depth) in a transitional region between relatively eutrophic waters to the north and oligotrophic subtropical waters to the south. The area is also the site of the Bermuda-Atlantic Times Series (BATS, Steinberg et al., 2001) and the Bermuda Testbed Mooring (BTM, Dickey et al., 2001). At the time of sample collection (May 2002), the mixed layer at OFP was ~30 m deep (van Beek et al., 2007).

The DYFAMED sediment trap time-series mooring was initiated in 1988 and is located in the north-western Mediterranean Sea (43°25' N; 7°52' E). It is situated in 2,350 m of water, approximately 45 km south of Cape Ferrat, France. The DYFAMED station is generally considered to be representative of open ocean conditions (Marty et al., 2002), although it may be episodically impacted by continental inputs (Sternberg et al., 2008; van Beek et al., 2009). It receives significant atmospheric input from the Saharan Desert (Sarthou and Jeandel, 2001). Between the two visits of the DYFAMED station considered here (BARMED 2 in March 2003 and BARMED 4 in May 2003), the mixed layer shoaled from ~25 m in March to ~15 m in May (van Beek et al., 2009).

Station A3-2 is located in the Indian sector of the Southern Ocean on the Kerguelen Plateau, south-east of the Kerguelen Islands and south of the Polar Front (Blain et al., 2007; Sanial et al., 2015). Following a first occupation during the KEOPS1 project in 2005 (PI: Stéphane Blain), this station was visited again in year 2011, in the framework of the KEOPS2 project (PI: Stéphane Blain). It is located in the HNLC (High Nutrient, Low Chlorophyll) waters of the Southern Ocean in water depth of 520 m. The Kerguelen Plateau was shown to deliver significant amounts of iron that promote an annual phytoplankton bloom in the region (Blain et al., 2007; van Beek et al., 2008). The mixed layer at station A3-2 was ~150 m deep when the samples were collected (Jouandet et al., 2014).

Finally, we report data from nine stations visited during the GEOVIDE cruise (GEOTRACES GA01) in the subpolar North Atlantic. The stations occupied during GEOVIDE present large differences in biogeochemical and hydrological properties (García-Ibáñez et al., 2018; Lemaitre et al., 2018b; Sarthou et al., 2018; Zunino et al., 2017). Stations 1 and 13 are located in the Iberian basin (on and west of the Iberian margin, respectively) and were occupied during the decline of a phytoplankton bloom. Several stations visited during GA01 are located in the vicinity of the North Atlantic Current, which flows in the West European basin (station 21) and in the Iceland basin (station 32 in the southern part of the basin, station 38 in the northern part), where nutrient availability and/or light limit primary production. West of these stations, along GA01, stations 44 and 51/60 in the Irminger Sea and stations 69 and 77 in the Labrador Sea were also sampled for ^{7}Be analysis. For this study, stations 51 and 60 are grouped as station 51/60 because these two stations are a cross-over station visited two days apart. Samples dedicated to particulate ^{7}Be analysis were collected at station 51 (on June 16) while those dedicated to total ^{7}Be analysis were collected two days later at station 60 (Shelley et al., 2017). The mixed layer depth (MLD), as estimated from density and temperature profiles

(Tonnard et al., 2018), ranged from ~12 m at stations 60 and 77 to ~48 m at station 51. The mixed layer at station 51/60 thus shoaled considerably between the two occupations, which was perhaps due to variability of the East Greenland Current and/or the Irminger Current (Daniault et al., 2011). Circulation patterns and water masses along GA01 are detailed in García-Ibáñez et al. (2018) and Zunino et al. (2017).

4. Results

4.1. $^{7}Be_{p}$ in the Sargasso Sea, Mediterranean Sea, and Kerguelen Plateau

The $^{7}Be_{p}$ activities determined on samples collected in the Sargasso Sea, Mediterranean Sea, and Kerguelen Plateau are given in Table 1 and shown in Figure 2. Overall, the $^{7}Be_{p}$ activities determined on mixed layer samples vary by one order of magnitude across these oceanic regions, from 3.0 dpm/m^{3} in the Mediterranean Sea at 15 m (DYFAMED, BARMED 2), to 25.2 dpm/m^{3} in the Sargasso Sea at 20 m (OFP). In the Southern Ocean (station A3-2), $^{7}Be_{p}$ activity is found to be ~12 dpm/m^{3} for the shallowest sample (40 m) and is comparable at the two other depths sampled in the mixed layer (average $^{7}Be_{p}$ activity of ~10 dpm/m^{3}). Significant temporal variations in surface water $^{7}Be_{p}$ activity are observed at station DYFAMED, with a much higher value in May 2003 (BARMED 4; 11.07 dpm/m^{3}) than in March 2003 (BARMED 2; 2.95 dpm/m^{3}; Figure 2). These variations may reflect (i) variations in MLD, which was shallower in May (~15 m) compared to March (~25 m), resulting in a greater dilution of ^{7}Be activities in March, and (ii) the greater stratification of the upper water column in May (van Beek et al., 2009), resulting in abated turbulent mixing with thermocline waters in May. Other factors may also be involved. Similar seasonal variations in total ^{7}Be were observed in other oceanic regions, such as in the Sargasso Sea, and were mainly ascribed to MLD variations (Kadko, 2009): the deeper the mixed layer, the lower the ^{7}Be activity as a result of dilution.

Noticeably, at the four stations in the Sargasso Sea, Mediterranean Sea, and Kerguelen Plateau, $^{7}Be_{p}$ activities are lower in the upper thermocline than in the mixed layer (Figure 2). This pattern is consistent with the atmospheric origin and the relatively short half-life of ^{7}Be. The vertical profiles generally show a monotonic decrease of $^{7}Be_{p}$ activity with depth below the mixed layer (Figure 2).

Station	Depth (m)	$^{7}Be_{p}$ (dpm/m^{3})		
OFP Time-series (Sargasso Sea, May 2002)				
OFP	20	25.16	±	2.05
OFP	70	5.30	±	0.80
OFP	120	1.96	±	0.41
OFP	300	0.47	±	0.13
OFP	700	0.12	±	0.08
OFP	1420	0.04	±	0.09
OFP	4250	0.05	±	0.09
BARMED 2 (DYFAMED, Mediterranean Sea, March 2003)				
DYFAMED	15	2.95	±	0.09
DYFAMED	50	2.03	±	0.05
DYFAMED	100	2.09	±	0.06
DYFAMED	185	0.54	±	0.02
DYFAMED	400	0.23	±	0.05
DYFAMED	600	0.13	±	0.05
DYFAMED	1000	0.06	±	0.06
BARMED 4 (DYFAMED, Mediterranean Sea, May 2003)				
DYFAMED	10	11.07	±	0.80
DYFAMED	50	4.55	±	0.38
DYFAMED	112	0.56	±	0.08
DYFAMED	140	0.32	±	0.08
DYFAMED	240	0.78	±	0.15
DYFAMED	400	0.37	±	0.06
DYFAMED	600	0.32	±	0.07
DYFAMED	2200	0.15	±	0.04
KEOPS2 (Indian sector of the Southern Ocean, November 2011)				
A3-2	40	12.31	±	1.00
A3-2	100	7.44	±	0.62
A3-2	150	10.92	±	0.76
A3-2	190	10.36	±	0.59
A3-2	230	3.49	±	0.35
A3-2	300	1.12	±	0.21
A3-2	400		BDL	
A3-2	460	0.66	±	0.19

Table 1: Particulate ^{7}Be activities (in dpm/m^{3}) determined at stations OFP (Sargasso Sea), DYFAMED (Mediterranean Sea), and A3-2 (Kerguelen Plateau). Versapor filters (0.8 µm) were used at stations OFP and DYFAMED, and Supor filters (0.8 µm) at station A3-2. The reported errors are standard deviations from the counting statistics. BDL: Below Detection Limit.

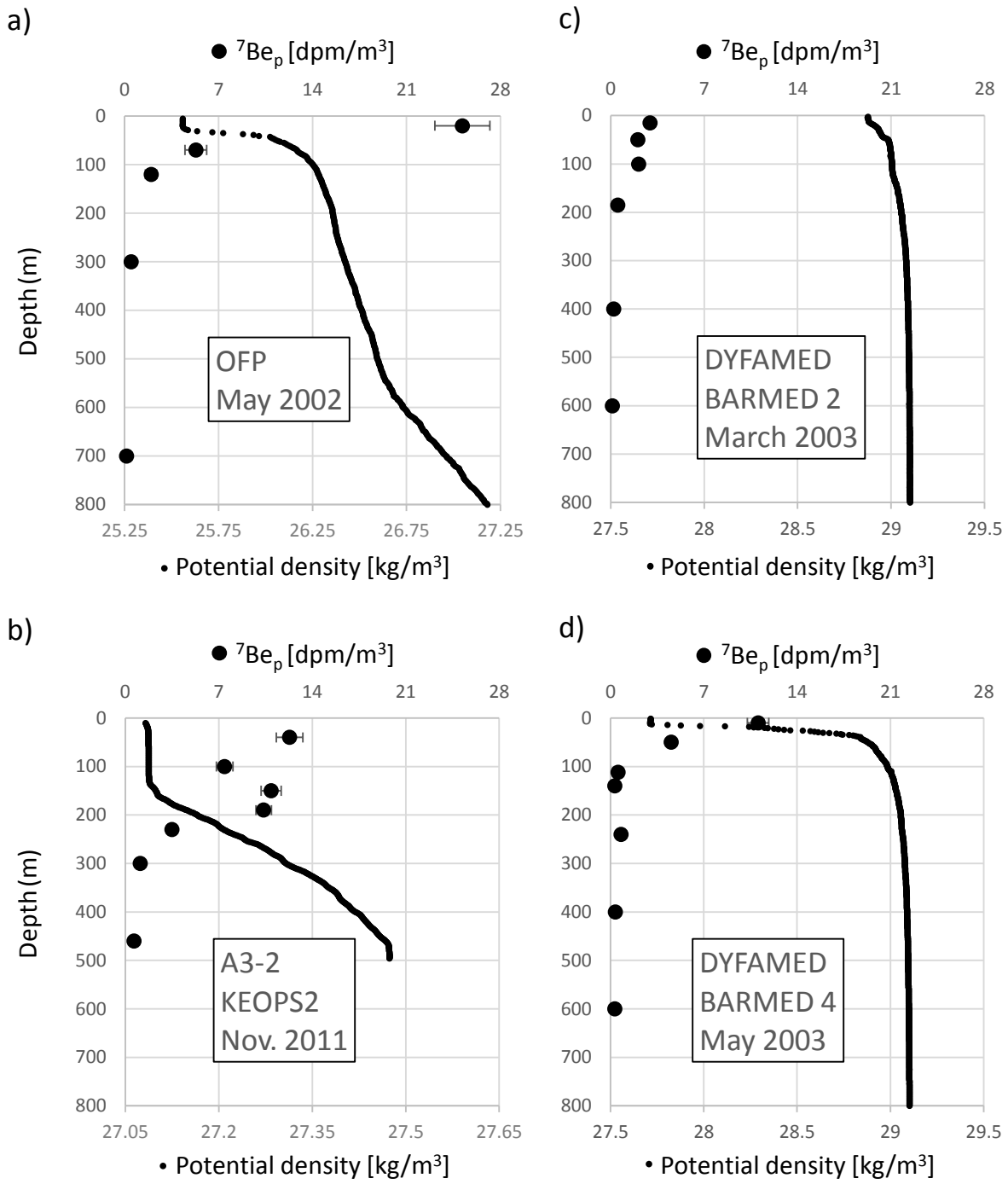

Figure 2: Profiles of particulate ^{7}Be activity (^7Be_p, in dpm/m^3; black dots) determined in suspended particles collected using *in situ* pumps at stations OFP (Sargasso Sea), DYFAMED (Mediterranean Sea), and A3-2 (Kerguelen Plateau). Error bars represent +/- 1 standard deviation from the counting statistics. Versapor filters of 0.8 µm pore size were used at all depths for OFP and BARMED cruises, whereas Supor filters of 0.8 µm pore size were used at all depths for KEOPS2 (Table 1). Potential density profiles from CTD cast data are also shown (small black dots).

4.2. Impact of the use of different filter types on ^7Be_p measurement

In contrast to stations OFP, DYFAMED, and A3-2, $^{7}Be_{p}$ measurements at different depths were obtained for samples collected from different filter types at GEOVIDE stations. These filter types include 1-µm pore size sock filters for surface waters (5 m) and 1-µm pore size QMA and 0.8-µm pore size Supor filters for deeper waters.

The use of different filter types may generate systematic differences in the determination of the $^{7}Be_{p}$ activities and thus produce artifacts in the $^{7}Be_{p}$ vertical profiles. To our knowledge, the impact of different filter types on the measurement of particulate Be concentration in seawater has never been examined. Most relevant to this issue is perhaps the study of Maiti et al. (2012), who compared particulate ^{234}Th activities of samples collected on QMA and Supor filter punches. The inter-filter variability was found to be 8.1% for QMA filter punches and 16.8% for Supor ones. For both filter types (QMA and Supor), inter-filter variability (i.e., the variability associated with subsamples taken from the same filter) in $^{234}Th_{p}$ was partly due to (i) an uneven distribution of particles on the filter and (ii) a potential bias associated with subsampling the particulate material on the filters (Maiti et al., 2012). In the present study, we did not analyze punches but the entire filter, so inter-filter variability associated with factor (i) above should not be a source of variability in our $^{7}Be_{p}$ dataset.

It was also shown that QMA filters may adsorb dissolved ^{234}Th, leading to ^{234}Th activities which are 10 to 20% higher on QMA filters (filtered volume: 450-600 L) than on Supor filters (filtered volume: 200-400 L; Maiti et al., 2012). Other studies, however, showed that the sorption effect tends to be larger for smaller sample volumes (Benitez-Nelson et al., 2001; Buesseler et al., 1998); for filtered volumes smaller than 150 L, ^{234}Th activities were found to be at least twice as high on QMA filters than on Nuclepore filters (Benitez-Nelson et al., 2001). In the present study, the volumes of seawater that was pumped through the QMA filters varied from 200 L to 850 L, while the volumes of seawater that passed through the 1-µm socks via the ship seawater intake varied from 1,200 L to 10,800 L (see Table 2). To our knowledge, this study is the first to report ^{7}Be activities of particulate material collected by 1-µm pore size socks, so that previous values are not available for comparison.

In order to estimate the impact of different filter types on the determination of $^{7}Be_{p}$, preliminary tests have been conducted on particulate samples collected near the Mediterranean coast. Surface seawater samples were collected in June 2022 aboard the R/V *Nereis II* at station POLA (42° 28’ 300” N, 03° 15’ 500” E; water depth: 95 m), located five miles offshore of Banyuls-sur-Mer. The samples were filtered in duplicate through the different types of filters

used during GEOVIDE: 0.8-µm pore size Supor filters, 1-µm pore size QMA filters, and 1-µm pore size socks.

We found that (i) the mean activity of $^{7}Be_{p}$ on 1-µm QMA filters (59.6 $\pm$ 1.7 dpm/m^{3}) was 2.1 times higher than the mean activity on 0.8-µm Supor filters (28.6 $\pm$ 1.4 dpm/m^{3}), and (ii) the mean activity of $^{7}Be_{p}$ on 1-µm sock filters (20.4 $\pm$ 2.2 dpm/m^{3}) was 1.4 times lower than the mean activity on 0.8-µm Supor filters (Figure 3). The activity differences far exceeded the errors associated with the counting statistics. Supor filters are considered here as a reference since they are the filters of choice for GEOTRACES (Maiti et al., 2012). In our tests, the seawater volume that passed through each filter was ~200 L, except for 0.8-µm Supor filters, which got clogged for smaller volumes (Figure 3). Although our tests are preliminary, they do suggest that dissolved ^{7}Be absorbs onto QMA filters, thus increasing the measured $^{7}Be_{p}$ activity, similarly to ^{234}Th (Maiti et al., 2012).

As noted above, we also found that a significant fraction of the particulate ^{7}Be is not recovered during the filtration through sock filters compared to Supor filters. This lower recovery for the sock filters is consistent with our results at GEOVIDE station 77, where the $^{7}Be_{p}$ activity determined at 5 m on 1-µm sock (6.54 dpm/m^{3}) is lower than the $^{7}Be_{p}$ activity determined at 10 m on 0.8-µm Supor filter (12.76 dpm/m^{3}; Table 2), although natural variability could also contribute to the difference.

In summary, our preliminary tests suggest that $^{7}Be_{p}$ activities on QMA and sock filters may show systematic difference with the $^{7}Be_{p}$ activities on the (reference) Supor filters. Here the results from these tests are used to correct the $^{7}Be_{p}$ activities on QMA and sock filters at GEOVIDE stations. The $^{7}Be_{p}$ activities on QMA filters are divided by 2.1, whereas the $^{7}Be_{p}$ activities on sock filters are multiplied by 1.4 (Table 2). The errors in the corrected $^{7}Be_{p}$ activities on QMA and sock filters are calculated by propagating the errors in the uncorrected activities and the errors in the correction factors, neglecting error covariances (Bevington and Robinson, 1992).

It is clear that the filter corrections applied to the $^{7}Be_{p}$ activities measured on QMA and sock filters are not without limitations. The correction factor applied to $^{7}Be_{p}$ activities on QMA filters for > 400 L of filtered seawater (see Table 2) may be overestimated if the sorption effect is smaller for larger sample volumes, as was observed for ^{234}Th (Maiti et al., 2012). Other effects, such as the concentration and the chemical composition of the particulate material may also contribute to the differences in $^{7}Be_{p}$ activity measured on different filter types. It is

therefore unclear whether filter corrections determined from one oceanographic environment (e.g., station POLA) could be applied to other stations (e.g., GEOVIDE stations). Nevertheless, we feel that the correction factors reported above for QMA and sock filters are currently the best approach to estimate the vertical distribution of $^{7}Be_{p}$ activity at GEOVIDE stations, where different filters were used at different depths.

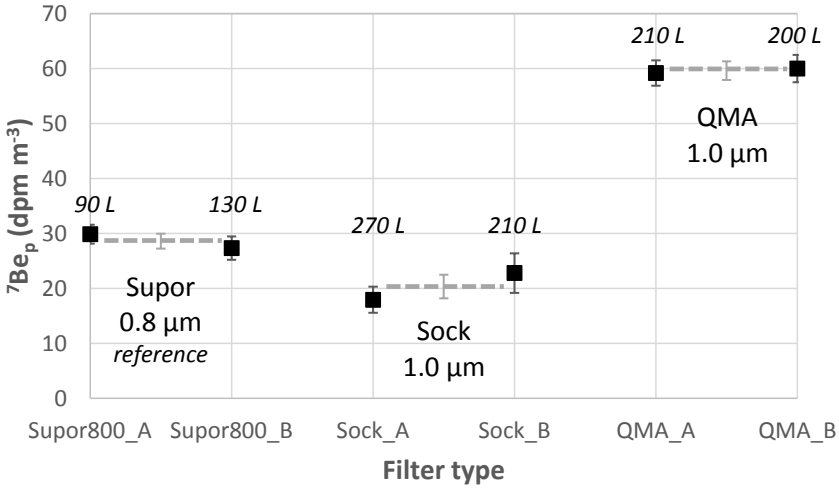

Figure 3: Preliminary tests of the impact of different filter types on the determination of $^{7}Be_{p}$ activity in seawater samples. Surface samples from station POLA were filtered through the different filters used at GEOVIDE stations (Supor 0.8 µm, Sock 1.0 µm, and QMA 1.0 µm). Duplicates were done for each filter (A and B; see filtered volume above each symbol) and gave reproducible $^{7}Be_{p}$ for each filter type (within +/- 1 standard deviation of each individual $^{7}Be_{p}$ measurement, derived from counting statistics). The grey dashed lines and associated error bars show, respectively, the mean $^{7}Be_{p}$ for each filter type and its uncertainty (error propagation).

Station	Depth (m)	Filter	Filtered volume (L)	Uncorrected $^{7}Be_{p}$ (dpm/m^{3})	Corrected $^{7}Be_{p}$ (dpm/m^{3})	$^{7}Be_{tot}$ (dpm/m^{3})*	Particulate fraction (%)
GEOVIDE (North Atlantic Ocean, May-June 2014)							
1	5	**1 µm sock**	10166	4.27 ± 0.93	**5.99 ± 1.48**	350 ± 30	**2**
13	5	**1 µm sock**	10815	BDL	BDL	150 ± 30	
21	5	**1 µm sock**	4768	BDL	BDL	144 ± 18	
32	5	**1 µm sock**	2899	BDL	BDL	210 ± 20	
38	5	**1 µm sock**	6534	3.02 ± 0.84	**4.24 ± 1.28**	152 ± 19	**3**
44	5	**1 µm sock**	2677	8.34 ± 1.80	**11.72 ± 2.87**	130 ± 20	**9**
44	40	0.8 µm Supor	297	1.16 ± 0.35	1.16 ± 0.35		
44	80	0.8 µm Supor	428	BDL	BDL		
44	150	0.8 µm Supor	740	BDL	BDL		
44	300	0.8 µm Supor	425	BDL	BDL		
51/60	5	**1 µm sock**	1191	12.32 ± 1.35	**17.32 ± 2.77**	195 ± 18	**9**
51/60	20	**1 µm QMA**	196	68.85 ± 3.21	**33.05 ± 3.94**	104 ± 14	**32**
51/60	70	**1 µm QMA**	586	18.64 ± 1.11	**8.95 ± 1.12**	53 ± 7	**17**

51/60	150	**1 µm QMA**	467	7.27 ± 0.94	**3.49 ± 0.59**	40 ± 7	**9**
69	5	**1 µm sock**	3277	11.60 ± 0.83	**16.29 ± 2.22**	180 ± 20	**9**
69	20	**1 µm QMA**	262	49.60 ± 1.72	**23.82 ± 2.74**	182 ± 8	**13**
69	30	0.8 µm Supor	162	2.52 ± 0.84	2.52 ± 0.84		
69	60	0.8 µm Supor	280	BDL	BDL		
69	70	**1 µm QMA**	481	5.87 ± 0.54	**2.82 ± 0.40**	43 ± 7	**7**
69	100	0.8 µm Supor	453	BDL	BDL	BDL	
77	5	**1 µm sock**	2349	4.65 ± 0.54	**6.54 ± 1.08**	212 ± 17	**3**
77	10	0.8 µm Supor	105	12.76 ± 1.28	12.76 ± 1.28		
77	20	**1 µm QMA**				112 ± 8	
77	45	**1 µm QMA**	842	4.42 ± 0.28	**2.12 ± 0.27**		
77	70	**1 µm QMA**	560	4.92 ± 0.39	**2.36 ± 0.32**	83 ± 6	**3**
77	149	**1 µm QMA**	761	2.29 ± 0.26	**1.10 ± 0.17**		
77	200	0.8 µm Supor	511	BDL	BDL		

*Shelley et al. (2017)

Table 2: Particulate and total activities of ^{7}Be ($^{7}Be_{p}$, $^{7}Be_{tot}$, in dpm/m^{3}) at GEOVIDE stations. Filter types and filtered volume are also specified. Particulate activities (uncorrected and corrected following filter types used) are reported (see Section 4.2). Total activities are from Shelley et al. (2017). The particulate fraction (%) refers to the ratio between the corrected particulate ^{7}Be and total ^{7}Be activities. BDL: Below Detection Limit.

4.3. $^{7}Be_{p}$ in the subpolar North Atlantic Ocean (GEOVIDE)

As observed for the other oceanic areas of the study, the $^{7}Be_{p}$ activity (corrected from the filter biases as defined in Section 4.2; Table 2 and Figure 4) is higher in the mixed layer than below at the GEOVIDE stations. At 5-m depth, the $^{7}Be_{p}$ activity varies from below the detection limit in the Iberian, West European and south Iceland basins (stations 13, 21, and 32, respectively) to ~17 dpm/m^{3} near the southern tip of Greenland in the western Irminger Sea and in the central Labrador Sea (respectively, station 51/60 and station 69). The $^{7}Be_{p}$ activity reaches 33 dpm/m^{3} and 24 dpm/m^{3} at 20 m at stations 51/60 and 69, respectively, in the lower part of the mixed layer (Table 2 and Figure 4). Note that the filter correction reduces, but does not completely suppress, the apparent $^{7}Be_{p}$ activity maximum observed in the lower part of the mixed layer (Figure 4). Below the mixed layer, the $^{7}Be_{p}$ activity generally drops to a maximum of ~3 dpm/m^{3}, similarly to what is observed in the other oceanic areas of the study.

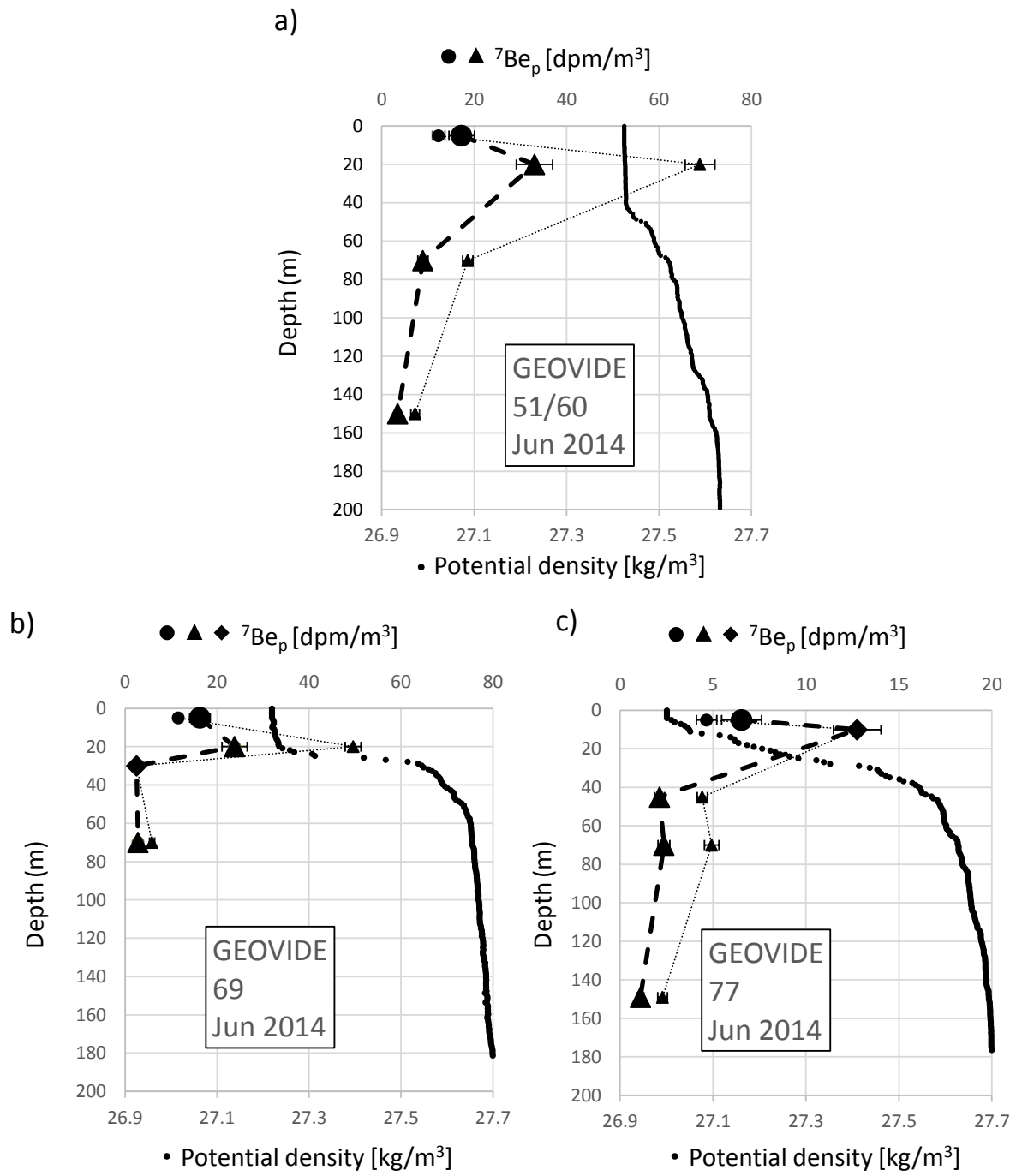

Figure 4: Profiles of particulate ^{7}Be activity ($^{7}Be_p$, in dpm/m^3) at GEOVIDE stations (uncorrected $^{7}Be_p$: small symbols and thin dotted line; corrected $^{7}Be_p$: large symbols and thick dashed line). Samples filtered through 1-µm pore size socks are identified by circles, 1-µm QMA filters by triangles, and 0.8-µm Supor filters by diamonds. Error bars for uncorrected activities represent +/- 1 standard deviation (counting statistics). Error bars for corrected activities are calculated by propagating the errors in the uncorrected activities and the errors in the filter corrections. Note that the x-axis range for $^{7}Be_p$ is smaller for station 77. The potential density profile from CTD cast data is also shown for each station (in kg/m^3; small dots).

5. Discussion

5.1. Comparison to previous $^{7}Be_{p}$ measurements

In this section, we compare the particulate ^{7}Be activities reported here with previous data from the literature (Figure 5 and Table 3). Silker et al. (1968) reported $^{7}Be_{p}$ activities ranging from below the detection limit (< 10 dpm/1000 L) to 70 dpm/1000 L in surface waters (2-20 m) of the Atlantic and Pacific oceans. Silker (1972a) published vertical profiles of ^{7}Be in the upper 100 m of the Atlantic Ocean and concluded that less than 10% of the measured radioactivity (i.e., < 90 dpm/m^3) was found in the insoluble fraction. Similar findings were reported in surface waters of the North Pacific (Silker, 1972b; < 65 dpm/m^3). Andrews et al. (2008) pumped ~1000 L of surface water from the Sargasso Sea through a 1-µm Hytrex filter and found that the $^{7}Be_{p}$ activity was below the detection limit (< 35 dpm/m^3). Kadko and Johns (2011) reported $^{7}Be_{p}$ activities in the mixed layer (between 7 and 18 m depth) in the equatorial Atlantic, with values ranging from below the detection limit (< 60 dpm/m^3) to 180 dpm/1000 L. Finally, Kremenchutskii et al. (2021) determined the $^{7}Be_{p}$ activity of samples collected in the Black Sea in the upper 65 m of the water column. The $^{7}Be_{p}$ values from that study ranged from 11 to 41 dpm/m^3 in surface (3 m) waters, from 10 to 11 dpm/m^3 between 15 and 18 m, and were below the detection limit (< 10 dpm/m^3) between 20 and 65 m.

Overall, the $^{7}Be_{p}$ activities reported in this study are of the same orders of magnitude as $^{7}Be_{p}$ activities reported in most previous studies (< 70 dpm/m^3; Kremenchutskii et al., 2021; Silker et al., 1968), although all are noticeably lower than the value of 180 dpm/m^3 observed in the equatorial Atlantic (Kadko and Johns, 2011; Figure 5). The $^{7}Be_{p}$ decrease with depth that is generally observed in this study is also qualitatively consistent with previous measurements in the Black Sea (Kremenchutskii et al., 2021). It is worth noting that, in the study of Kadko and Johns (2011), particle samples were collected by passing 200 L of seawater through GF/F filters made of borosilicate glass, a material which was shown to retain dissolved ^{234}Th, as for QMA quartz filters (Benitez-Nelson et al., 2001). Our preliminary tests show that $^{7}Be_{p}$ activities measured on QMA filters significantly exceed $^{7}Be_{p}$ activities measured on reference Supor filters (section 4.2), which suggests that the $^{7}Be_{p}$ activities of equatorial Atlantic samples reported in Kadko and Johns (2011) may be overestimated.

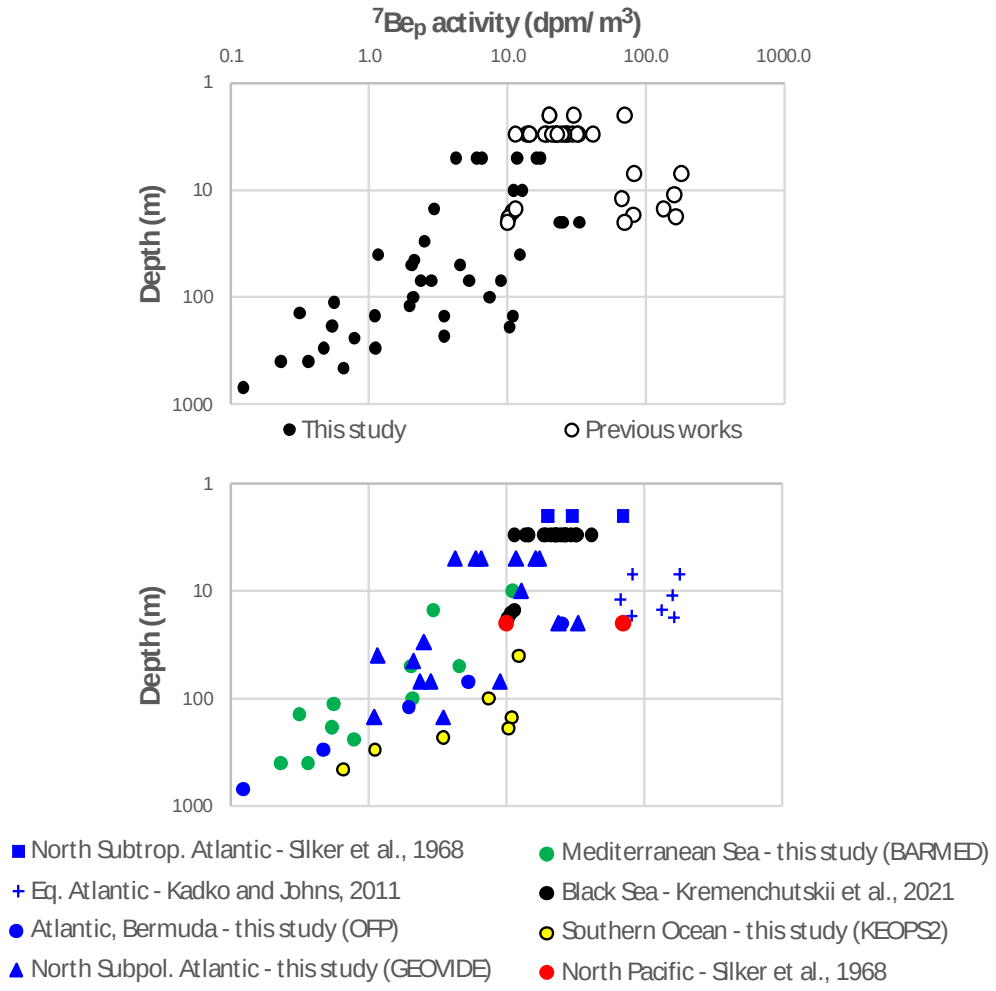

457

458 **Figure 5:** Compilation of open ocean $^{7}Be_p$ data (in dpm/m^3, log scale) as a function of depth (in m, log
459 scale). Top panel shows previous data (open circles) and those from this study (black dots). Bottom
460 panel shows different oceanic areas: the Atlantic Ocean (blue), the Mediterranean Sea (green), the Black
461 Sea (black), the Southern Ocean (yellow), and the North Pacific (red).

462

Location	Sampled depths (m)	Filtration method	Material	Porosity (µm)	Diameter (mm)	Volume filtered (L)	$^{7}Be_p$ range (dpm m^{-3})	$^{7}Be_p/^{7}Be_{tot}$ range (%)	Reference
North Atlantic	2	Millipore filtration unit	Plastic	0.3	305	1000-5000	20-70	6-15	Silker et al. (1968)
North Pacific	20	Millipore filtration unit	Plastic	0.3	305	1000-5000	10-70	4-24	Silker et al. (1968)
NW Atlantic	0-97	Millipore filtration unit	Glass	0.3	305?	not specified	<5-10%	NA	Silker (1972)
Sargasso Sea	3	HYTREX filter	Polypropylene	1	NA	1000	BDL	NA	Andrews et al. (2008)
Eq. Atlantic	7-18	GF/F filter	Borosilicate glass	not specified	142	200	70-180	18-38	Kadko and Johns (2011)
Black Sea	3-18	Aquafilter FCPS1	Polypropylene	1	NA	2000-10000	10-40	5-13	Kremenchutskii et al. (2021)
Med. Sea	10-2200	Versapor	Acrylic copolymer	0.8	142	200-2400	0.1-11.1	NA	This study

Sargasso Sea	20-4250	Versapor	Acrylic copolymer	0.8	142	100-2300	0.1-25.2	NA	This study
Southern Ocean	40-460	Supor	Hydrophilic polyethersulfone	0.8	142	100-300	0.7-12.3	NA	This study
North Atlantic	5	Pentek BP-410-1	Polypropylene	1	NA	1000-10000	4-17	2-9	This study
	>5-150	Supor	Hydrophilic polyethersulfone	0.8	142	100-300	1-13	NA	
	>5-150	QMA	Quartz	1	142	200-800	1-33	3-32	

*NA: not applicable

Table 3: Characteristics of $^{7}Be_{p}$ sampling methods and range of $^{7}Be_{p}$ values obtained in previous studies and in this study.

5.2. Are the oceanic $^{7}Be_{p}$ activities significant?

By combining the corrected $^{7}Be_{p}$ activities at GEOVIDE stations and the total ^{7}Be activities at the same stations, at the same depths, but from different casts (Shelley et al., 2017), the fraction of total ^{7}Be that is bound to suspended particles can be tentatively estimated. From this approach, we find that the particulate fraction would account for 2-9% of the total ^{7}Be activity at a water depth of 5 m (n = 6), 13-32% at 20 m (n = 2), and 3-17% at 70 m (n = 3; Table 2; Figures 6 and 7). Note that at station 77, the highest $^{7}Be_{p}$ activity is observed at 10 m (Supor filter), at a depth where $^{7}Be_{tot}$ was not determined (Table 2). Considering the $^{7}Be_{tot}$ activity determined either at 5 m or 20 m (respectively, above and below the depth of the particulate sample), we find that the particulate fraction would amount to 6 or 11%, respectively, in agreement with the values reported above. These fractions are similar to those estimated for surface waters in (i) the North Atlantic at 2 m (6-15%; Silker et al., 1968, using 0.3-µm pore size filters; Table 3), (ii) the Black Sea between 3 and 18 m (5-13%; Kremenchutskii et al., 2021, using 1-µm pore size filters), (iii) the North Pacific at 20 m (4-24%; Silker et al., 1968), and (iv) the equatorial Atlantic between 7 and 18 m (18-38%; Kadko and Johns, 2011; Figure 7).

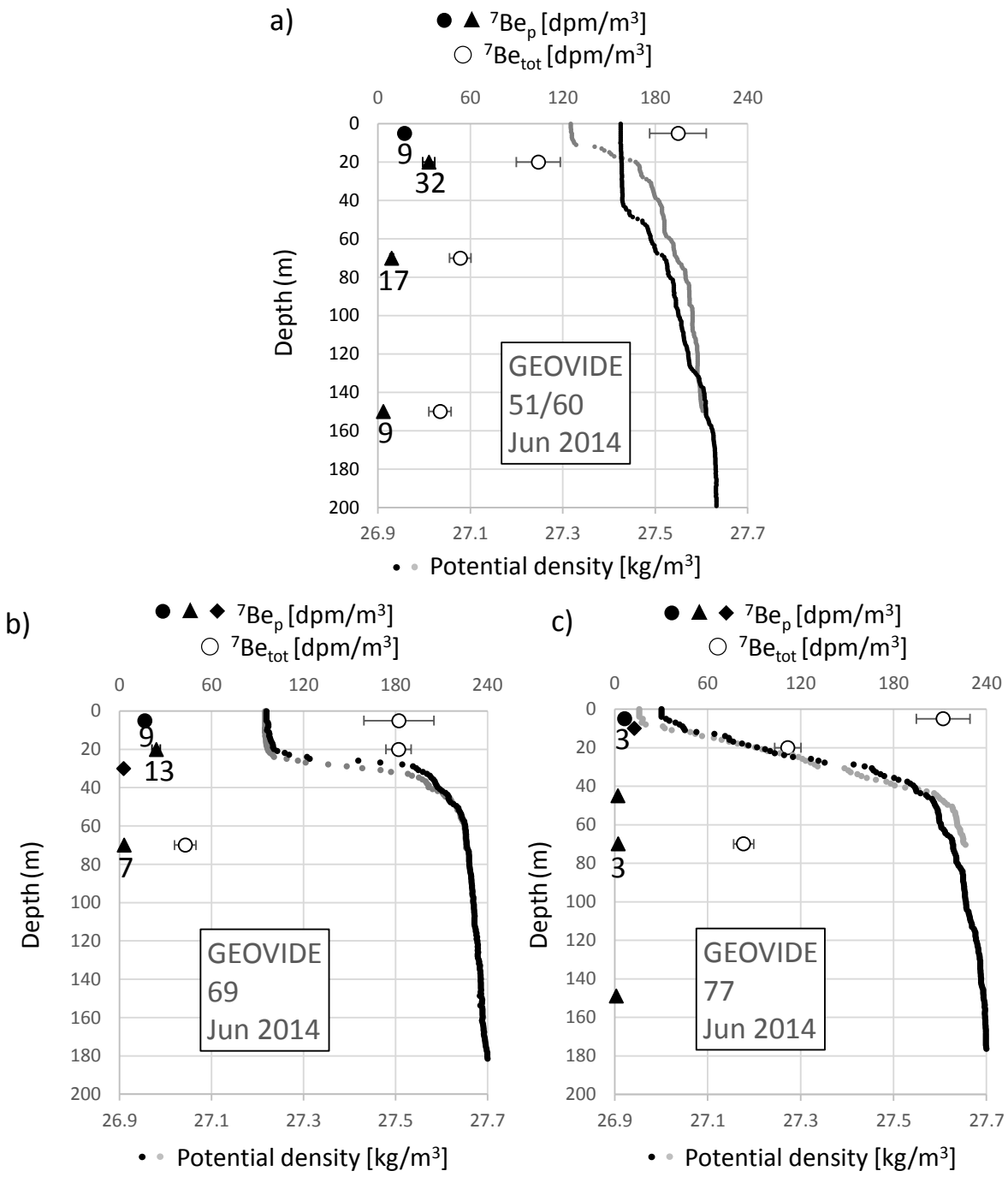

Figure 6: Profiles of corrected particulate ^{7}Be activity ($^{7}Be_{p}$, in dpm/m^{3}; solid symbols) and total ^{7}Be activity ($^{7}Be_{tot}$, in dpm/m^{3}; open circles; Shelley et al., 2017) at GEOVIDE stations. For $^{7}Be_{p}$, samples filtered through 1-µm pore size socks are identified by circles, 1-µm QMA filters by triangles, and 0.8-µm Supor filters by diamonds. Numbers below data points are the ratio of particulate ^{7}Be to total ^{7}Be (in %). Error bars for the corrected $^{7}Be_{p}$ are calculated by propagating the errors in the uncorrected $^{7}Be_{p}$ and the errors in the filter corrections. Potential density profiles from CTD cast data are also shown for each station (in kg/m^{3}; small grey dots for the cast associated with $^{7}Be_{tot}$ sample collection, small black dots for $^{7}Be_{p}$).

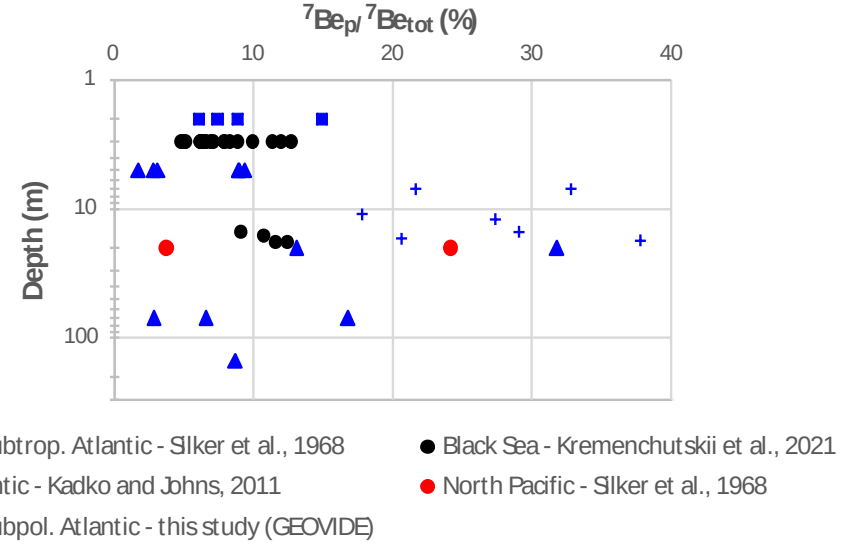

Figure 7: Compilation of estimates of the $^{7}Be_p/^{7}Be_{tot}$ activity ratio in the open ocean (in %, linear scale) as a function of depth (in m, log scale). Data from the Atlantic Ocean are in blue, in black for the Black Sea, and in red for the North Pacific Ocean.

To further assess the significance of the ^{7}Be particulate fraction in comparison to the dissolved fraction, we calculate the inventory (vertical integral) of $^{7}Be_p$ activity at stations where inventories of total ^{7}Be activities were reported in the literature (i.e., at the OFP and GEOVIDE stations). $^{7}Be_p$ inventories are calculated by integrating the $^{7}Be_p$ activities at the different sampling depths using the trapezoidal formula. For this calculation, we assume that (i) $^{7}Be_p$ activity at the surface (z = 0 m) is equal to the activity determined at the shallowest sampling depth and (ii) $^{7}Be_p$ activity is 0 dpm/m^3 at 1500 m at OFP and is 0 dpm/m^3 at the maximum sampling depth at GEOVIDE stations (see Table 4; Shelley et al., 2017). At all stations, the error in the $^{7}Be_p$ inventory is estimated by propagating the errors in the individual $^{7}Be_p$ measurements (Bevington and Robinson 1992).

At the OFP station, we find that the $^{7}Be_p$ inventory amounts to 1830 ± 340 dpm/m^2, which represents only about 5% of the total ^{7}Be inventory of ~40,000 dpm/m^2 at this station (Aaboe et al., 1981; Kadko et al., 2015; Kadko and Prospero, 2011; Silker, 1972b).

The $^{7}Be_p$ inventories at the GEOVIDE stations 51/60, 69 and 77 vary significantly, ranging from 530 ± 70 dpm/m^2 at station 77 to 2060 ± 270 dpm/m^2 at station 51/60, while $^{7}Be_{tot}$ inventories are comparable at these three stations (~10,000 dpm/m^2; Shelley et al., 2017). The errors of 70 and 270 dpm/m^2 reflect the uncertainties in the $^{7}Be_p$ measurements and in the filter

biases (Bevington and Robinson, 1992). The ratio of $^{7}Be_{p}$ inventory to total ^{7}Be inventory varies therefore widely across the GEOVIDE stations, from 5% at station 77 to up to 19% at station 51/60 (Table 4). The upper end of this range (19%) should be considered with caution, considering that it results from $^{7}Be_{tot}$ and $^{7}Be_{p}$ activities estimated from samples from different casts under different hydrographic conditions (Station 51/60). A number of factors that could explain the wide range are discussed in the following subsections.

Station	^{7}Be inventory depth range* [m]	$^{7}Be_{tot}$ inventory* [dpm/m^2]	**$^{7}Be_{p}$ inventory [dpm/m^2]**	**Relative $^{7}Be_{p}$ inventory [%]**	$^{7}Be_{tot}$ flux* [dpm/m^2/d]	**$^{7}Be_{p}$ flux [dpm/m^2/d]**
51/60	0-175	11000 ± 300	**2060 ± 270**	**19 ± 2**	143 ± 4	**27 ± 4**
69	0-87	9700 ± 300	**640 ± 90**	**7 ± 1**	126 ± 4	**8 ± 1**
77	0-150	10500 ± 300	**530 ± 70**	**5 ± 1**	136 ± 4	**7 ± 1**

*Shelley et al. (2017)

Table 4: Inventories of $^{7}Be_{tot}$ (in dpm/m^2) and corrected $^{7}Be_{p}$ (in dpm/m^2 and in % of $^{7}Be_{tot}$) at GEOVIDE stations 51/60, 69, and 77, and equivalent surface fluxes from atmospheric deposition (in dpm/m^2/d). $^{7}Be_{tot}$ water column inventories and surface fluxes are from Shelley et al. (2017).

5.3. Which processes shape the vertical profiles of $^{7}Be_{p}$?

The higher $^{7}Be_{p}$ activities in the ocean mixed layer than below that are found in this study are consistent with the combined effects of atmospheric deposition and radioactive decay. The decrease in $^{7}Be_{p}$ activity with depth below the mixed layer (Figures 2 and 6) is expected to result, at least partly, from radioactive decay, as is the case for $^{7}Be_{tot}$ (Silker, 1972b, 1972a). One can wonder, however, if other processes may also influence the vertical distribution of $^{7}Be_{p}$ in the upper ocean. Since Be is a particle-reactive element, exchanges of ^{7}Be between the dissolved and particulate phases may occur and impact the vertical distribution of $^{7}Be_{p}$ as well as the $^{7}Be_{p}$ inventory in the water column. In order to assess whether processes other than surface deposition impact the $^{7}Be_{p}$ activities measured during GEOVIDE, we compare the $^{7}Be_{p}$ deposition fluxes estimated from aerosol samples collected during GEOVIDE (Shelley et al., 2017) with $^{7}Be_{p}$ deposition flux estimated from our $^{7}Be_{p}$ inventories.

Shelley et al. (2017) estimated surface $^{7}Be_{tot}$ deposition fluxes from $^{7}Be_{tot}$ inventories determined in the water column, following a method which assumes that the only loss of ^{7}Be from the water column is radioactive decay (Kadko et al. 2015). A similar method is applied here for $^{7}Be_{p}$ deposition. It assumes that (i) $^{7}Be_{p}$ is supplied to the ocean only via atmospheric deposition (dry deposition + particulate fraction of wet deposition), (ii) no particulate ^{7}Be is lost in the water column by particle degradation (dissolution and/or remineralization) or by desorption, and (iii) no particulate ^{7}Be is gained in the water column by adsorption of dissolved

545 ^{7}Be onto particles (scavenging). Collectively, assumptions (i)-(iii) imply that, at steady state,
546 the flux of $^{7}Be_{p}$ at the sea surface from atmospheric deposition is balanced by the $^{7}Be_{p}$ decay
547 rate integrated over the water column.

548 The above method gives atmospheric deposition fluxes of $^{7}Be_{p}$ of 27 dpm/m^{2}/d at station
549 51/60, 8 dpm/m^{2}/d at station 69, and 7 dpm/m^{2}/d at station 77 (Table 4). These fluxes are
550 compared below to the dry deposition fluxes of $^{7}Be_{p}$ that have been derived at these stations
551 from the analysis of aerosols sampled on the ship during GEOVIDE (Shelley et al., 2017).

552 Consider first the comparison for stations 69 and 77. Our estimates of $^{7}Be_{p}$ deposition are
553 two to three times lower than those derived from aerosols for station 69 (25 dpm/m^{2}/d) and
554 station 77 (16 dpm/m^{2}/d; Table 2 of Shelley et al., 2017). Several factors could explain the
555 discrepancies between the $^{7}Be_{p}$ deposition flux estimated from aerosols and from $^{7}Be_{p}$
556 inventories in the water column. They are similar to those discussed by Shelley et al. (2017) in
557 their effort to explain the discrepancies between estimates of $^{7}Be_{tot}$ deposition based on (i)
558 precipitation and aerosol samples collected on the ship and (ii) $^{7}Be_{tot}$ inventories in the water
559 column.

560 For example, the dry ^{7}Be fluxes estimated during GEOVIDE were obtained from the
561 analysis of aerosols sampled during short periods of time (~2 days; Shelley et al., 2017).
562 Estimates of dry ^{7}Be deposition based on measurements collected over a period of few days
563 may not be adequate to interpret measurements of ^{7}Be activity in the water column, which
564 should integrate the collective effects of surface inputs extending over several months. The
565 different time scales characterizing aerosol sampling and the evolution of ^{7}Be in the water
566 column could explain why the estimates of $^{7}Be_{p}$ deposition derived from $^{7}Be_{p}$ water column
567 inventories are different than those derived from ship data (Shelley et al., 2017), although why
568 the former are lower than the latter remains unclear (see below).

569 At least three other factors could be responsible for the relatively low $^{7}Be_{p}$ deposition flux
570 estimated from $^{7}Be_{p}$ inventory at stations 69 and 77. A first factor is a loss of ^{7}Be from the
571 particulate phase to the dissolved phase owing to the dissolution of aerosols in the upper water
572 column. A second factor is the downward export of particulate ^{7}Be to depth due to some
573 combination of particle aggregation and gravitational settling. Evidence of high POC export at
574 stations 69 and 77 is provided by the observation of strong ^{234}Th disequilibria with its
575 radioactive parent (Lemaitre et al., 2018a). Shelley et al. (2017) reported that ^{7}Be deposition
576 fluxes derived from water column $^{7}Be_{tot}$ inventories are generally lower than ^{7}Be deposition

fluxes from precipitation at GEOVIDE stations (their Table 2), and they also suggested that the discrepancy could be explained by scavenging of ^{7}Be onto sinking particles. A third factor is the overestimation of the dry deposition velocity assumed by Shelley et al. (2017). In this earlier study, a deposition velocity of 0.3 cm/s was assumed, but the authors acknowledged that the relative error in this parameter could be up to 300%.

We now compare the estimate of $^{7}Be_p$ surface flux based on $^{7}Be_p$ water column inventory with that based on aerosol data at station 51/60. The ^{7}Be activity in the aerosol sample collected near station 51/60 was below the detection limit (Shelley et al., 2017), while it is at this station that we estimate the highest atmospheric deposition flux from the $^{7}Be_p$ inventory (27 dpm/m^2/d) among stations 51/60, 69 and 77. The higher $^{7}Be_p$ surface flux deduced from the $^{7}Be_p$ inventory compared to that deduced from aerosol data near station 51/60 could also be due to a number of factors. These include, again, the different time scales captured by the atmospheric and oceanic samples, but also the adsorption of dissolved ^{7}Be onto particles, and a significant source of particulate ^{7}Be from wet deposition, which is unaccounted for in the calculation of dry $^{7}Be_p$ deposition from ship data. On this note, precipitation events did occur near station 51/60 during the first half of May, 2014 (see Shelley et al., 2017; their Figure S5).

5.4. Exchange of ^{7}Be between the dissolved and particulate phases

It is instructive to consider the $^{7}Be_p$ activities per mass of particles in order to assess how the $^{7}Be_p$ activities at GEOVIDE stations relate to particle concentrations. The $^{7}Be_p$ activities per volume of water are divided by the suspended particle matter concentrations ([SPM]; Figure 8) to derive specific $^{7}Be_p$ activities (in dpm per gram of particles) at these stations. Interestingly, at station 51/60, the specific $^{7}Be_p$ activities below the mixed layer (70 and 150 m) are similar to that in the mixed layer (20 m), whereas the $^{7}Be_p$ activities (per volume of water) are significantly lower below the mixed layer than at 20 m (SPM concentrations were not determined at station 77). Thus, the amount of ^{7}Be bound to particles per mass of particles is approximately the same in the mixed layer and in the upper thermocline.

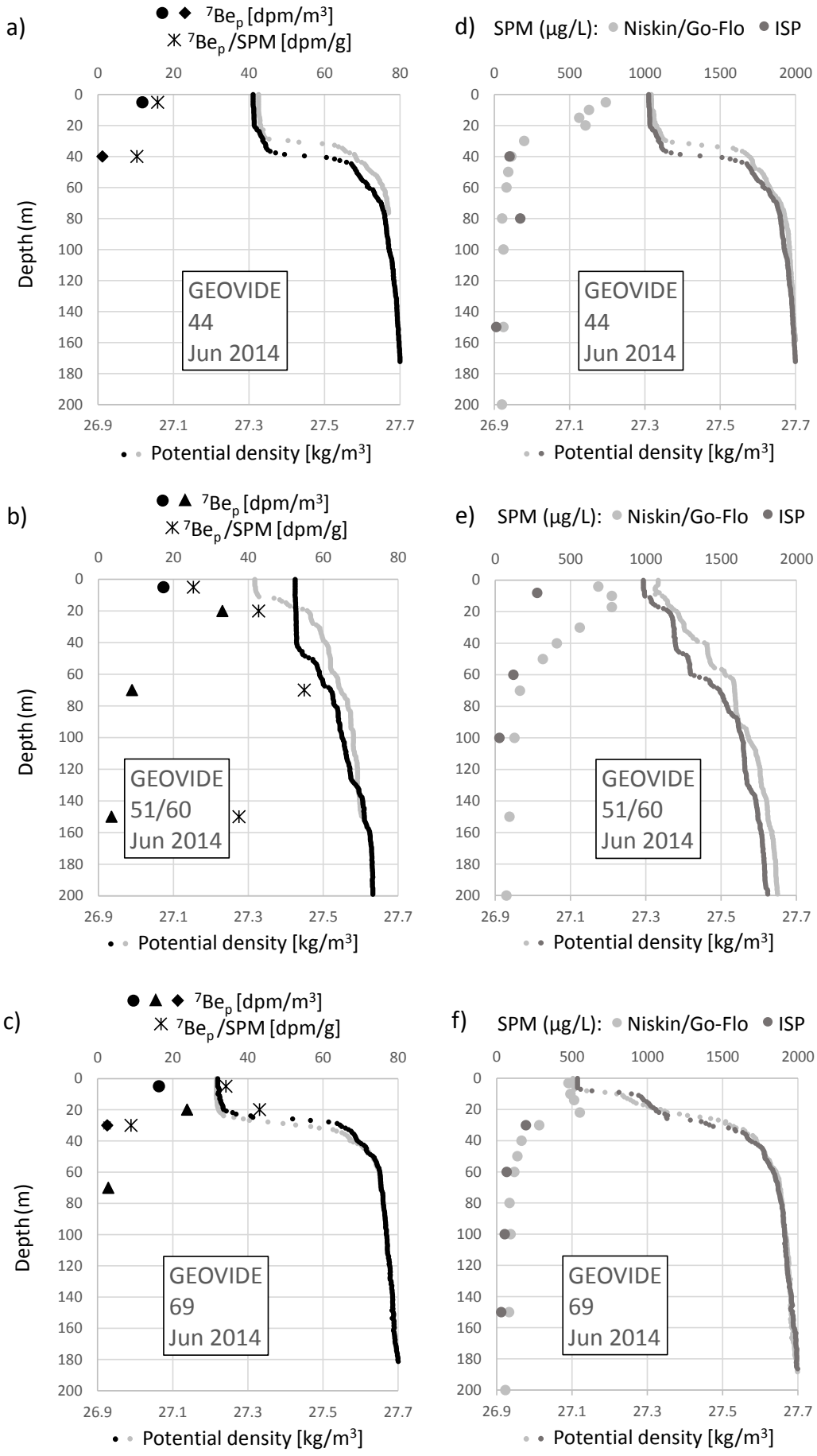
a)
^7Be_p [dpm/m^3]
^7Be_p/SPM [dpm/g]
Depth (m)
GEOVIDE
44
Jun 2014
Potential density [kg/m^3]
d)
SPM (µg/L): Niskin/Go-Flo ISP
GEOVIDE
44
Jun 2014
Potential density [kg/m^3]
b)
^7Be_p [dpm/m^3]
^7Be_p/SPM [dpm/g]
Depth (m)
GEOVIDE
51/60
Jun 2014
Potential density [kg/m^3]
e)
SPM (µg/L): Niskin/Go-Flo ISP
GEOVIDE
51/60
Jun 2014
Potential density [kg/m^3]
c)
^7Be_p [dpm/m^3]
^7Be_p/SPM [dpm/g]
Depth (m)
GEOVIDE
69
Jun 2014
Potential density [kg/m^3]
f)
SPM (µg/L): Niskin/Go-Flo ISP
GEOVIDE
69
Jun 2014
Potential density [kg/m^3]

605

606 **Figure 8:** (left panels) Profiles of $^{7}Be_{p}$ (in dpm/m^3; black markers: circles for 1-µm pore size sock
607 samples, triangles for 1-µm QMA filter samples, diamonds for 0.8-µm Supor filters, with filter
608 corrections applied) and $^{7}Be_{p}$/SPM (in dpm/g; asterisks) at GEOVIDE stations (a) 44, (b) 51/60, and (c)
609 69. Potential density profiles from CTD cast data are also shown (in kg/m^3; small grey dots for the cast
610 associated with $^{7}Be_{tot}$ sample collection, small black dots for $^{7}Be_{p}$). (right panels) Profiles of suspended
611 particulate matter concentration (SPM, in µg/L) at GEOVIDE stations (d) 44, (e) 51/60, and (f) 69,
612 determined from particles collected using Niskin or Go-Flo bottles (Lagarde et al., submitted; light grey
613 dots) and *in situ* pumps (ISP; Tang et al., 2018; dark grey dots), together with their associated potential
614 density profiles (in kg/m^3; small dots).

615

616 We combine the measurements of particulate ^{7}Be, total ^{7}Be, and SPM which are available
617 at GEOVIDE stations to derive tentative estimates of the distribution coefficient for ^{7}Be:

618 $$K_d = \frac{[\,^{7}Be_p]}{[\,^{7}Be_d] \times [SPM]} \quad (1)$$

619 Here [$^{7}Be_{d}$] is the activity of ^{7}Be in the dissolved phase, deduced from the difference between
620 total activity [$^{7}Be_{tot}$] (Shelley et al., 2017) and corrected particulate activity [$^{7}Be_{p}$] (see Table
621 2). The distribution coefficient K_d quantifies the solid/solution partitioning of the nuclide in the
622 water column: a higher value of K_d indicates that a greater proportion of ^{7}Be is bound to
623 particles for the same amount of particles. SPM concentrations are expressed in g/cm^3 in order
624 to facilitate comparison to K_d values from previous studies (e.g., Baskaran et al., 1997; Chuang
625 et al., 2013). Thus, the K_d values reported in this paper are in cm^3/g. Estimates of logK_d (base
626 10) are reported in Table 5, together with SPM concentrations. Note that our K_d values should
627 be regarded as tentative estimates given that the concentrations of $^{7}Be_{p}$, $^{7}Be_{tot}$ and SPM
628 determined at GEOVIDE stations are generally for distinct casts and that, at some stations, these
629 casts exhibited different density profiles (Figure 8).

Station	**Depth (m)**	**SPM (10^{-9} g/cm^3)**	logK_d
1	5	111	5.19
38	5	261	5.04
44	5	741	5.14
51/60	5	684	5.15
51/60	20	773	5.78
51/60	70	163	6.09
51/60	150	93	6.01
69	5	477	5.30
69	20	553	5.51

630 **Table 5:** Suspended particulate matter concentration (SPM; in 10^{-9} g/cm^3) and tentative estimates of the
631 distribution coefficient K_d for ^{7}Be at GEOVIDE stations (expressed as $\log_{10}$ of K_d).

The $\log K_d$ values for GEOVIDE samples vary from 5.04 (surface sample; station 38) to 6.09 (70 m; station 60). They overlap with (i) values from 4.92 to 6.16 determined from ^{10}Be measurements from the Middle Atlantic Bight, the equatorial Pacific, and the Pacific sector of the Southern Ocean (Chase et al., 2002) and (ii) values from 5.04 to 5.30 determined from recent ^{7}Be measurements in the Black Sea (Kremenchutskii et al., 2021). On the other hand, they are higher, or slightly higher, than values between 3 and 5 obtained from samples collected at the OFP station (Chuang et al., 2013), in Tampa Bay (Florida, USA; Baskaran and Swarzenski, 2007), and in estuaries of the Sabine-Neche (Texas, USA) and the Loire (France; Baskaran et al., 1997; Ciffroy et al., 2003).

The distribution coefficient of a trace element in seawater can decrease with particle concentration, the so-called particle concentration effect (e.g., Honeyman and Santschi, 1988). The relatively large K_d values for ^{7}Be estimated at GEOVIDE stations may result from lower SPM concentrations (< 1 mg/L, as commonly found in open ocean waters; Guo et al., 1997), since previous K_d estimates for ^{7}Be mostly pertain to near-shore or estuarine waters. Lower K_d values are commonly observed in freshwater and estuarine environments, which are generally characterized by higher [SPM] (tens to thousands of mg/L; e.g. Baskaran and Santschi, 1993; Woźniak et al., 2010) than in open ocean waters, a pattern often attributed to the particle concentration effect (Benoit and Rozan, 1999; D. Tang et al., 2002). However, as observed in estuarine environments (e.g. Baskaran et al., 1997), the K_d values estimated at GEOVIDE stations do not show a significant correlation with [SPM] (Figure 9; $R^2 = 0.09$, p-value = 0.43). On the other hand, the $\log K_d$ values at GEOVIDE stations show a clear difference between surface and deep waters: they amount to 5.2 ± 0.1 (average $\pm$ 1 standard deviation) for surface samples (5 m) and 6.1 ± 0.1 for the deepest samples (70-150 m). This difference in $\log K_d$ between surface and deep waters suggests that a higher fraction of dissolved ^{7}Be is found in the particulate phase in deep waters than in surface waters, when differences in particle concentration are taken into account. Note, however, that for station 51/60, the particulate fraction at each depth may be biased because $^{7}Be_p$ and $^{7}Be_{tot}$ were measured at different times under different hydrographic conditions (Figure 6a).

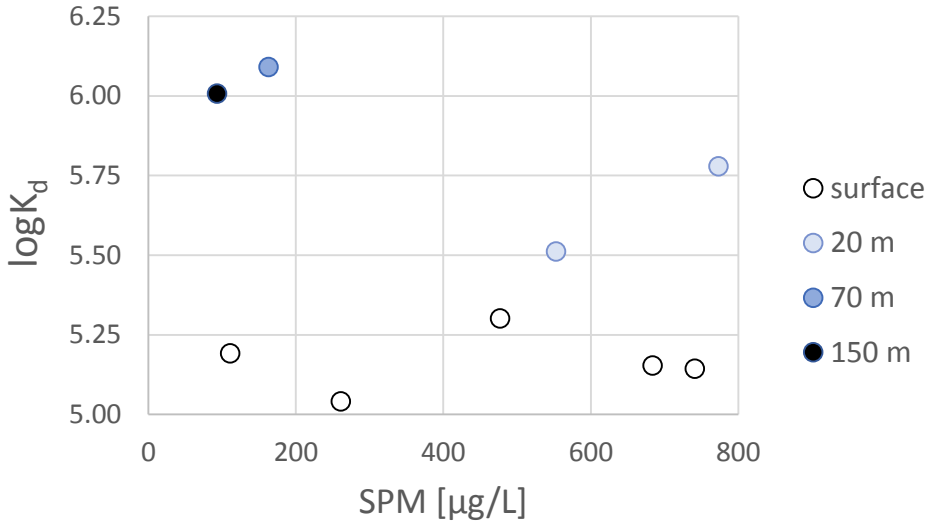

Figure 9: Distribution coefficient for ^{7}Be ($\log K_d$), as a function of SPM concentrations at GEOVIDE stations. The distribution coefficient could be determined only for stations and depths where [SPM], particulate ^{7}Be activity, and total ^{7}Be activity were all determined (see Table 5). $^{7}Be_d$ activities were determined by difference (total ^{7}Be minus corrected particulate ^{7}Be).

6. Conclusions

The purpose of this study is to better assess the significance of particulate ^{7}Be ($^{7}Be_p$) in the oceanic cycle of ^{7}Be and for the use of ^{7}Be as a tracer of atmospheric inputs and dynamical processes in the upper water column. Using low-background gamma-ray spectrometers operating in underground facilities, we produce relatively precise measurements of ^{7}Be activity in suspended particles collected in four different oceanic regions: the subpolar North Atlantic, the Sargasso Sea, the western Mediterranean Sea, and the Indian sector of the Southern Ocean. At three stations in the subpolar North Atlantic (GEOVIDE stations), we consider our results in the light of published measurements of total ^{7}Be activity, estimates of $^{7}Be_p$ deposition, and estimates of particulate matter concentration, yielding insights into the solid-solution partitioning of ^{7}Be and into other aspects of the oceanic cycle of ^{7}Be.

We find that, in each oceanic region, the $^{7}Be_p$ activity generally decreases with depth, with maxima in the mixed layer and minima in the thermocline. The trend is particularly robust at stations where the particulate samples dedicated to ^{7}Be have been collected by filtration through the same filter type at all depths (stations OFP, DYFAMED, and A3-2). Preliminary tests based on particulate samples collected at a near-coastal site in the western Mediterranean Sea, show that $^{7}Be_p$ measured on QMA filters and polypropylene filters are, respectively, greater and smaller than $^{7}Be_p$ measured on the Supor filters used in GEOTRACES. Results from these tests

688 are used to apply filter-specific corrections to the $^{7}Be_{p}$ measurements at GEOVIDE stations,
689 where measurements of total ^{7}Be activity are also available but where QMA and polypropylene
690 filters were used to collect the particulate material at different depths.

691 We find that, at GEOVIDE stations, in agreement with previous studies, the corrected $^{7}Be_{p}$
692 activity accounts for less than 10% of the total ^{7}Be activity in surface waters (water depth of 5
693 m; 6% on average, n = 6) and for a larger proportion of total ^{7}Be in the lower part of the mixed
694 layer (20 m; 22% on average, n = 2). Below the mixed layer, in the thermocline, the corrected
695 $^{7}Be_{p}$ fraction generally also accounts for less than 10% (70 m; 9% on average, n = 3). The
696 corrected $^{7}Be_{p}$ is estimated to represent 5-19% of the total ^{7}Be inventory in the water column,
697 suggesting that the amount of ^{7}Be bound to particles is small but not insignificant.

698 Evidence gathered at GEOVIDE stations suggests that ^{7}Be bound to marine particles may
699 not originate exclusively from atmospheric deposition. The $^{7}Be_{p}$ deposition fluxes derived from
700 water column inventories are noticeably lower, or higher (depending on location), than those
701 derived from the $^{7}Be_{p}$ activity of aerosols and an assumed dry deposition velocity. Differences
702 could be explained by (i) the different time scales captured by the atmospheric and oceanic
703 samples, (2) the uncertainty in the dry deposition velocity, (3) an unaccounted significant source
704 of particulate ^{7}Be from wet deposition, (4) adsorption of dissolved ^{7}Be onto particulate matter,
705 and/or (5) a release of particulate ^{7}Be into solution. Shelley et al. (2017) also pointed out, from
706 a comparison between different deposition estimates, that water column scavenging of ^{7}Be
707 could have been significant at some GEOVIDE stations.

708 Evidence at GEOVIDE stations also suggests that the sorptive properties of particles with
709 respect to ^{7}Be may be different in the mixed layer and in the thermocline. Distribution
710 coefficients of ^{7}Be at these stations are estimated to be systematically higher in the thermocline
711 than in the mixed layer. Although the coefficient estimates suffer from relatively large
712 uncertainties, due in particular to differences in sampling, they do suggest that a larger fraction
713 of ^{7}Be occurs in the particulate phase in the thermocline, when differences in particle
714 concentration between surface and deep waters are considered.

715 The results reported in this paper support the notion that ^{7}Be may undergo an exchange
716 between the dissolved and particulate phases in the ocean. However, the implications of these
717 findings for the use of ^{7}Be as a tracer of oceanic processes and surface deposition are unclear.
718 The assumptions underlying the use of ^{7}Be as a tracer of oceanic and surface processes depend
719 not only on the affinity of ^{7}Be for marine particles, but also on the magnitude of particulate ^{7}Be

export to the deep ocean compared to radioactive decay. Future research should thus focus on quantifying the downward export of $^{7}Be_{p}$ to deep waters, and on assessing its temporal and spatial variability. The variability of the $^{7}Be_{p}$ and $^{7}Be_{d}$ pools should also be assessed in order to investigate how inventories vary with time and space. A better understanding of the temporal and spatial variability of (wet and dry) ^{7}Be deposition to the sea surface is also needed. Moreover, our results raise the necessity to further assess the influence of different filter types on the measurement of $^{7}Be_{p}$ activity in oceanic samples. Finally, future sampling programs should aim to collect seawater and particulate samples at the same locations, at the same depths, and at the same time. Using the present dataset, a companion paper further explores the significance of particle scavenging and export for the cycling of ^{7}Be in the ocean (Lerner et al., in preparation).

Acknowledgements

We are grateful to the crews and captains of *Weatherbird II* (OFP, Bermuda), *Téthys II* (DYFAMED), *Marion Dufresne* (KEOPS2), *Pourquoi Pas ?* (GEOVIDE), and *Nereis II* (POLA, off Banyuls-sur-Mer). We thank Maureen Conte (PI OFP program), Catherine Jeandel (PI of the BARMED project), Stéphane Blain (PI of the KEOPS2 project), Géraldine Sarthou and Pascale Lherminier (PIs of the GEOVIDE project). We wish to acknowledge Maureen Conte (Bermuda), Claudie Marec (DYFAMED), Fabien Pérault, Bruno Lansard, and Ester Garcia-Solsona (KEOPS2) for their help during ISP deployments. We also acknowledge Emmanuel de Saint Léger, Fabien Pérault, Frédéric Planchon, Hélène Planquette, Yi Tang, Maxi Castrillejo, Nolwenn Lemaître, and Catherine Jeandel for their help during ISP deployment during GEOVIDE. We are grateful to Pierre Branellec, Floriane Desprez de Gésincourt, Michel Hamon, Catherine Kermabon, Philippe Le Bot, Stéphane Leizour, Olivier Ménage, Fabien Pérault, and Emmanuel de Saint-Léger for their technical support during the GEOVIDE expedition. We are grateful to Cyann Paque, Laurent Zudaire and Renaud Vuillemin for technical help during the cruise conducted off Banyuls-sur-Mer. We thank Frédéric Planchon for sharing QMA filters for the cruise conducted off Banyuls-sur-Mer. Finally, we thank Thomas Zambardi at the LAFARA underground laboratory as well as Charlotte Riccio, Thierry Sampieri, Jean-Louis Saury and Aurélien Rojas at the underground laboratory of Modane (LSM). We acknowledge support by the French National program LEFE (Les Enveloppes Fluides et l'Environnement) funded by CNRS-INSU (BE-7-FLUX). We thank the

three anonymous reviewers and associate editor for their constructive comments that allowed us to improve significantly the quality of the manuscript.

References

Aaboe, E., Dion, E.P., Turekian, K.K., 1981. 7 Be in Sargasso Sea and Long Island Sound waters . J. Geophys. Res. 86, 3255. https://doi.org/10.1029/jc086ic04p03255

Andrews, J.E., Hartin, C., Buesseler, K.O., 2008. 7Be analyses in seawater by low background gamma-spectroscopy. J. Radioanal. Nucl. Chem. 277, 253–259. https://doi.org/10.1007/s10967-008-0739-y

Baskaran, M., Ravichandran, M., Bianchi, T.S., 1997. Cycling of 7Be and 210Pb in a high DOC, shallow, turbid estuary of south-east Texas. Estuar. Coast. Shelf Sci. 45, 165–176. https://doi.org/10.1006/ecss.1996.0181

Baskaran, M., Santschi, P.H., 1993. The role of particles and colloids in the transport of radionuclides in coastal environments of Texas. Mar. Chem. 43, 95–114. https://doi.org/10.1016/0304-4203(93)90218-D

Baskaran, M., Swarzenski, P.W., 2007. Seasonal variations on the residence times and partitioning of short-lived radionuclides (234Th, 7Be and 210Pb) and depositional fluxes of 7Be and 210Pb in Tampa Bay, Florida. Mar. Chem. 104, 27–42. https://doi.org/10.1016/j.marchem.2006.06.012

Benitez-Nelson, C.R., Buesseler, K.O., Van Der Loeff, M.R., Andrews, J., Ball, L., Crossin, G., Charette, M.A., 2001. Testing a new small-volume technique for determining 234Th in seawater. J. Radioanal. Nucl. Chem. 248, 795–799. https://doi.org/10.1023/A:1010621618652

Benoit, G., Rozan, T.F., 1999. The influence of size distribution on the particle concentration effect and trace metal partitioning in rivers. Geochim. Cosmochim. Acta 63, 113–127. https://doi.org/10.1016/S0016-7037(98)00276-2

Bevington, P.R., Robinson, D.K., 1992. Data Reduction and Error Analysis for the Physical Sciences, 2nd ed. WCB/McGraw-Hill, New York.

Blain, S., Quéguiner, B., Armand, L., Belviso, S., Bombled, B., Bopp, L., Bowie, A., Brunet, C., Brussaard, C., Carlotti, F., Christaki, U., Corbière, A., Durand, I., Ebersbach, F., Fuda, J.-L., Garcia, N., Gerringa, L., Griffiths, B., Guigue, C., Guillerm, C., Jacquet, S., Jeandel, C., Laan, P., Lefèvre, D., Lo Monaco, C., Malits, A., Mosseri, J., Obernosterer, I., Park, Y.-H., Picheral, M., Pondaven, P., Remenyi, T., Sandroni, V., Sarthou, G., Savoye, N., Scouarnec, L., Souhaut, M., Thuiller, D., Timmermans, K., Trull, T., Uitz, J., van Beek, P., Veldhuis, M., Vincent, D., Viollier, E., Vong, L., Wagener, T., 2007. Effect of natural iron fertilization on carbon sequestration in the Southern Ocean. Nature 446, 1070–1074. https://doi.org/10.1038/nature05700

Browne, E., Dairiki, J.M., Doebler, R.E., Shihab-Eldin, A., Jardine, L.J., Tuli, J.K., Buyrn, A.B., 1978. Table of isotopes, 7th ed. Wiley, New York.

Buesseler, K., Ball, L., Andrews, J., Benitez-Nelson, C., Belastock, R., Chai, F., Chao, Y., 1998. Upper ocean export of particulate organic carbon in the Arabian Sea derived from thorium-234. Deep. Res. Part II Top. Stud. Oceanogr. 45, 2461–2487. https://doi.org/10.1016/S0967-0645(98)80022-2

Burd, A.B., Jackson, G.A., 2009. Particle aggregation. Ann. Rev. Mar. Sci. 1, 65–90. https://doi.org/10.1146/annurev.marine.010908.163904

796 Chase, Z., Anderson, R.F., Fleisher, M.Q., Kubik, P.W., 2002. The Influence of Particle Composition
797 on Scavenging of Th, Pa and Be in the Ocean. Earth Planet. Sci. Lett. 204, 215–229.

798 Chuang, C.Y., Santschi, P.H., Ho, Y.F., Conte, M.H., Guo, L., Schumann, D., Ayranov, M., Li, Y.H.,
799 2013. Role of biopolymers as major carrier phases of Th, Pa, Pb, Po, and Be radionuclides in
800 settling particles from the atlantic ocean. Mar. Chem. 157, 131–143.
801 https://doi.org/10.1016/j.marchem.2013.10.002

802 Ciffroy, P., Reyss, J.L., Siclet, F., 2003. Determination of the residence time of suspended particles in
803 the turbidity maximum of the Loire estuary by 7Be analysis. Estuar. Coast. Shelf Sci. 57, 553–
804 568. https://doi.org/10.1016/S0272-7714(02)00339-6

805 Conte, M.H., Ralph, N., Ross, E.H., 2001. Seasonal and interannual variability in deep ocean particle
806 fluxes at the Oceanic Flux Program (OFP)/Bermuda Atlantic Time Series (BATS) site in the
807 western Sargasso Sea near Bermuda. Deep. Res. Part II Top. Stud. Oceanogr. 48, 1471–1505.
808 https://doi.org/10.1016/S0967-0645(00)00150-8

809 Dibb, J.E., Rice, D.L., 1989. Temporal and spatial distribution of beryllium-7 in the sediments of
810 Chesapeake Bay. Estuar. Coast. Shelf Sci. 28, 395–406. https://doi.org/10.1016/0272-
811 7714(89)90087-5

812 Dickey, T., Zedler, S., Yu, X., Doney, S.C., Frye, D., Jannasch, H., Manov, D., Sigurdson, D.,
813 McNeil, J.D., Dobeck, L., Gilboy, T., Bravo, C., Siegel, D.A., Nelson, N., 2001. Physical and
814 biogeochemical variability from hours to years at the Bermuda Testbed Mooring site: June 1994-
815 March 1998. Deep. Res. Part II Top. Stud. Oceanogr. 48, 2105–2140.
816 https://doi.org/10.1016/S0967-0645(00)00173-9

817 Feely, H.W., Larsen, R.J., Sanderson, C.G., 1989. Factors that cause seasonal variations in Beryllium-
818 7 concentrations in surface air. J. Environ. Radioact. 9, 223–249. https://doi.org/10.1016/0265-
819 931X(89)90046-5

820 Gaffney, J.S., Orlandini, K.A., Marley, N.A., Popp, C.J., 1994. Measurements of 7 Be and 210 Pb in
821 Rain, Snow, and Hail. J. Appl. Meteorol. 33, 869–873. https://doi.org/10.1175/1520-
822 0450(1994)033<0869:MOAIRS>2.0.CO;2

823 García-Ibáñez, M.I., Pérez, F.F., Lherminier, P., Zunino, P., Mercier, H., Tréguer, P., 2018. Water
824 mass distributions and transports for the 2014 GEOVIDE cruise in the North Atlantic.
825 Biogeosciences 15, 2075–2090. https://doi.org/10.5194/bg-15-2075-2018

826 Gourain, A., Planquette, H., Cheize, M., Lemaitre, N., Menzel Barraqueta, J.L., Shelley, R.,
827 Lherminier, P., Planquette, H., 2019. Inputs and processes affecting the distribution of particulate
828 iron in the North Atlantic along the GEOVIDE (GEOTRACES GA01) section. Biogeosciences
829 16, 1563–1582. https://doi.org/10.5194/bg-16-1563-2019

830 Guo, L., Santschi, P.H., Baskaran, M., 1997. Interactions of thorium isotopes with colloidal organic
831 matter in oceanic environments. Colloids Surfaces A Physicochem. Eng. Asp. 120, 255–271.
832 https://doi.org/10.1016/S0927-7757(96)03723-5

833 Haskell, W.Z., Kadko, D., Hammond, D.E., Knapp, A.N., Prokopenko, M.G., Berelson, W.M.,
834 Capone, D.G., 2015. Upwelling velocity and eddy diffusivity from 7Be measurements used to
835 compare vertical nutrient flux to export POC flux in the Eastern Tropical South Pacific. Mar.
836 Chem. 168, 140–150. https://doi.org/10.1016/j.marchem.2014.10.004

837 Honeyman, B.D., Santschi, P.H., 1988. Metals in aquatic systems. Environ. Sci. Technol. 22, 862–
838 871. https://doi.org/10.1021/es00173a002

839 Jouandet, M.P., Jackson, G.A., Carlotti, F., Picheral, M., Stemmann, L., Blain, S., 2014. Rapid
840 formation of large aggregates during the spring bloom of Kerguelen Island: Observations and
841 model comparisons. Biogeosciences 11, 4393–4406. https://doi.org/10.5194/bg-11-4393-2014

Kadko, D., 2017. Upwelling and primary production during the U.S. GEOTRACES East Pacific Zonal Transect. Global Biogeochem. Cycles 218–232. https://doi.org/10.1002/2016GB005554

Kadko, D., 2009. Rapid oxygen utilization in the ocean twilight zone assessed with the cosmogenic isotope 7 Be. Global Biogeochem. Cycles 23, n/a-n/a. https://doi.org/10.1029/2009GB003510

Kadko, D., Aguilar-Islas, A., Bolt, C., Buck, C.S., Fitzsimmons, J.N., Jensen, L.T., Landing, W.M., Marsay, C.M., Rember, R., Shiller, A.M., Whitmore, L.M., Anderson, R.F., 2019. The residence times of trace elements determined in the surface Arctic Ocean during the 2015 US Arctic GEOTRACES expedition. Mar. Chem. 208, 56–69. https://doi.org/10.1016/j.marchem.2018.10.011

Kadko, D., Aguilar-Islas, A., Buck, C.S., Fitzsimmons, J.N., Landing, W.M., Shiller, A., Till, C.P., Bruland, K.W., Boyle, E.A., Anderson, R.F., 2020. Sources, fluxes and residence times of trace elements measured during the U.S. GEOTRACES East Pacific Zonal Transect. Mar. Chem. 222. https://doi.org/10.1016/j.marchem.2020.103781

Kadko, D., Johns, W., 2011. Inferring upwelling rates in the equatorial Atlantic using 7Be measurements in the upper ocean. Deep Sea Res. Part I Oceanogr. Res. Pap. 58, 647–657. https://doi.org/10.1016/j.dsr.2011.03.004

Kadko, D., Landing, W.M., Shelley, R.U., 2015. A novel tracer technique to quantify the atmospheric flux of trace elements to remote ocean regions. J. Geophys. Res. Ocean. 120, 848–858. https://doi.org/10.1002/2014JC010314

Kadko, D., Olson, D., 1996. Beryllium-7 as a tracer of surface water subduction and mixed-layer history. Deep. Res. Part I Oceanogr. Res. Pap. 43, 89–116. https://doi.org/10.1016/0967-0637(96)00011-8

Kadko, D., Prospero, J., 2011. Deposition of 7Be to Bermuda and the regional ocean: Environmental factors affecting estimates of atmospheric flux to the ocean. J. Geophys. Res. Ocean. 116, 1–10. https://doi.org/10.1029/2010JC006629

Kremenchutskii, D.A., Batrakov, G.F., Dovhyi, I.I., Sapozhnikov, Y.A., 2021. Role of suspended matter in controlling beryllium-7 (7Be) in the Black Sea surface layer. J. Mar. Syst. 217. https://doi.org/10.1016/j.jmarsys.2021.103513

Lal, D., Peters, B., 1967. Cosmic Ray Produced Radioactivity on the Earth. pp. 551–612. https://doi.org/10.1007/978-3-642-46079-1_7

Lam, P.J., Ohnemus, D.C., Auro, M.E., 2015. Size-fractionated major particle composition and concentrations from the US GEOTRACES North Atlantic Zonal Transect. Deep. Res. Part II Top. Stud. Oceanogr. 116, 303–320. https://doi.org/10.1016/j.dsr2.2014.11.020

Lemaitre, N., Planchon, F., Planquette, H., Dehairs, F., Fonseca-Batista, D., Roukaerts, A., Deman, F., Tang, Y., Mariez, C., Sarthou, G., 2018a. High variability of particulate organic carbon export along the North Atlantic GEOTRACES section GA01 as deduced from 234Th fluxes. Biogeosciences 15, 6417–6437. https://doi.org/10.5194/bg-15-6417-2018

Lemaitre, N., Planquette, H., Planchon, F., Sarthou, G., Jacquet, S., García-Ibáñez, M.I., Gourain, A., Cheize, M., Monin, L., André, L., Laha, P., Terryn, H., Dehairs, F., 2018b. Particulate barium tracing of significant mesopelagic carbon remineralisation in the North Atlantic. Biogeosciences 15, 2289–2307. https://doi.org/10.5194/bg-15-2289-2018

Maiti, K., Buesseler, K.O., Pike, S.M., Benitez-Nelson, C., Cai, P., Chen, W., Cochran, K., Dai, M., Dehairs, F., Gasser, B., Kelly, R.P., Masque, P., Miller, L.A., Miquel, J.C., Moran, B.B., Morris, P.J., Peine, F., Planchon, F., Renfro, A.A., van der Loeff, M.R., Santschi, P.H., Turnewitsch, R., Waples, J.T., Xu, C., 2012. Intercalibration studies of short-lived thorium-234 in the water column and marine particles. Limnol. Oceanogr. Methods 10, 631–644. https://doi.org/10.4319/lom.2012.10.631

889 Martínez-Ruiz, F., Borrego, E., San Miguel, E.G., Bolívar, J.P., 2007. An efficiency calibration for
890 210Pb and 7Be measurements by gamma-ray spectrometry in atmospheric filters. Nucl.
891 Instruments Methods Phys. Res. Sect. A Accel. Spectrometers, Detect. Assoc. Equip. 580, 663–
892 666. https://doi.org/10.1016/j.nima.2007.05.117

893 Marty, J.C., Chiavérini, J., Pizay, M.D., Avril, B., 2002. Seasonal and interannual dynamics of
894 nutrients and phytoplankton pigments in the western Mediterranean Sea at the DYFAMED time-
895 series station (1991-1999). Deep. Res. Part II Top. Stud. Oceanogr. 49, 1965–1985.
896 https://doi.org/10.1016/S0967-0645(02)00022-X

897 Olsen, C.R., Larsen, I.L., Lowry, P.D., Cutshall, N.H., Nichols, M.M., 1986. Geochemistry and
898 deposition of 7Be in river-estuarine and coastal waters. J. Geophys. Res. 91, 896–908.
899 https://doi.org/10.1029/jc091ic01p00896

900 Papastefanou, C., Ioannidou, A., 1996. Influence of air pollutants in the 7be size distribution of
901 atmospheric aerosols. Aerosol Sci. Technol. 24, 102–106.
902 https://doi.org/10.1080/02786829608965355

903 Reyss, J.L., Schmidt, S., Legeleux, F., Bonté, P., 1995. Large, low background well-type detectors for
904 measurements of environmental radioactivity. Nucl. Inst. Methods Phys. Res. A 357, 391–397.
905 https://doi.org/10.1016/0168-9002(95)00021-6

906 Sanial, V., Van Beek, P., Lansard, B., Souhaut, M., Kestenare, E., D'Ovidio, F., Zhou, M., Blain, S.,
907 2015. Use of Ra isotopes to deduce rapid transfer of sediment-derived inputs off Kerguelen.
908 Biogeosciences 12, 1415–1430. https://doi.org/10.5194/bg-12-1415-2015

909 Sarthou, G., Jeandel, C., 2001. Seasonal variations of iron concentrations in the Ligurian Sea and iron
910 budget in the Western Mediterranean Sea. Mar. Chem. 74, 115–129.
911 https://doi.org/10.1016/S0304-4203(00)00119-5

912 Sarthou, G., Lherminier, P., Achterberg, E.P., Alonso-Pérez, F., Bucciarelli, E., Boutorh, J., Bouvier,
913 V., Boyle, E.A., Branellec, P., Carracedo, L.I., Casacuberta, N., Castrillejo, M., Cheize, M.,
914 Contreira Pereira, L., Cossa, D., Daniault, N., De Saint-Léger, E., Dehairs, F., Deng, F., Desprez
915 De Gésincourt, F., Devesa, J., Foliot, L., Fonseca-Batista, D., Gallinari, M., Garciá-Ibáñez, M.I.,
916 Gourain, A., Grossteffan, E., Hamon, M., Eric Heimbürger, L., Henderson, G.M., Jeandel, C.,
917 Kermabon, C., Lacan, F., Le Bot, P., Le Goff, M., Le Roy, E., Lefèbvre, A., Leizour, S.,
918 Lemaitre, N., Masqué, P., Ménage, O., Barraqueta, J.L.M., Mercier, H., Perault, F., Pérez, F.F.,
919 Planquette, H.F., Planchon, F., Roukaerts, A., Sanial, V., Sauzède, R., Schmechtig, C., Shelley,
920 R.U., Stewart, G., Sutton, J.N., Tang, Y., Tisnérat-Laborde, N., Tonnard, M., Tréguer, P., Van
921 Beek, P., Zurbrick, C.M., Zunino, P., 2018. Introduction to the French GEOTRACES North
922 Atlantic transect (GA01): GEOVIDE cruise. Biogeosciences 15, 7097–7109.
923 https://doi.org/10.5194/bg-15-7097-2018

924 Shelley, R.U., Roca-Martí, M., Castrillejo, M., Sanial, V., Masqué, P., Landing, W.M., van Beek, P.,
925 Planquette, H., Sarthou, G., 2017. Quantification of trace element atmospheric deposition fluxes
926 to the Atlantic Ocean (>40°N; GEOVIDE, GEOTRACES GA01) during spring 2014. Deep Sea
927 Res. Part I Oceanogr. Res. Pap. 119, 34–49. https://doi.org/10.1016/j.dsr.2016.11.010

928 Silker, W.B., 1972a. Horizontal and vertical distributions of radionuclides in the North Pacific Ocean.
929 J. Geophys. Res. 77, 1061–1070. https://doi.org/10.1029/JC077i006p01061

930 Silker, W.B., 1972b. Beryllium-7 and fission products in the Geosecs II water column and applications
931 of their oceanic distributions. Earth Planet. Sci. Lett. 16, 131–137. https://doi.org/10.1016/0012-
932 821X(72)90247-6

933 Silker, W.B., Robertson, D.E., Rieck, H.G., Perkins, R.W., Prospero, J.M., 1968. Beryllium-7 in ocean
934 water. Science (80-.). 161, 879–880. https://doi.org/10.1126/science.161.3844.879

935 Steinberg, D.K., Carlson, C.A., Bates, N.R., Johnson, R.J., Michaels, A.F., Knap, A.H., 2001.

936 Overview of the US JGOFS Bermuda Atlantic Time-series Study (BATS): A decade-scale look
937 at ocean biology and biogeochemistry. Deep. Res. Part II Top. Stud. Oceanogr. 48, 1405–1447.
938 https://doi.org/10.1016/S0967-0645(00)00148-X

939 Sternberg, E., Jeandel, C., Robin, E., Souhaut, M., 2008. Seasonal cycle of suspended barite in the
940 mediterranean sea. Geochim. Cosmochim. Acta 72, 4020–4034.
941 https://doi.org/10.1016/j.gca.2008.05.043

942 Tang, D., Warnken, K.W., Santschi, P.H., 2002. Distribution and partitioning of trace metals (Cd, Cu,
943 Ni, Pb, Zn) in Galveston Bay waters. Mar. Chem. 78, 29–45. https://doi.org/10.1016/S0304-
944 4203(02)00007-5

945 Tang, Y., Castrillejo, M., Roca-Martí, M., Masqué, P., Lemaitre, N., Stewart, G., 2018. Distributions
946 of total and size-fractionated particulate 210Po and 210Pb activities along the North Atlantic
947 GEOTRACES GA01 transect: GEOVIDE cruise. Biogeosciences 15, 5437–5453.
948 https://doi.org/10.5194/bg-15-5437-2018

949 Tonnard, M., Planquette, H., Bowie, A.R., van der Merwe, P., Gallinari, M., Desprez de Gésincourt,
950 F., Germain, Y., Gourain, A., Benetti, M., Reverdin, G., Tréguer, P., Boutorh, J., Cheize, M.,
951 Menzel Barraqueta, J.-L., Pereira-Contreira, L., Shelley, R., Lherminier, P., Sarthou, G., 2018.
952 Dissolved iron in the North Atlantic Ocean and Labrador Sea along the GEOVIDE section
953 (GEOTRACES section GA01). Biogeosciences Discuss. 1–53. https://doi.org/10.5194/bg-2018-
954 147

955 van Beek, P., Bourquin, M., Reyss, J.-L., Souhaut, M., Charette, M., Jeandel, C., 2008. Radium
956 isotopes to investigate the water mass pathways on the Kerguelen Plateau (Southern Ocean).
957 Deep Sea Res. Part II Top. Stud. Oceanogr. 55, 622–637.
958 https://doi.org/10.1016/j.dsr2.2007.12.027

959 van Beek, P., François, R., Conte, M., Reyss, J.L., Souhaut, M., Charette, M., 2007. 228Ra/226Ra and
960 226Ra/Ba ratios to track barite formation and transport in the water column. Geochim.
961 Cosmochim. Acta 71, 71–86. https://doi.org/10.1016/j.gca.2006.07.041

962 van Beek, P., Souhaut, M., Lansard, B., Bourquin, M., Reyss, J.L., von Ballmoos, P., Jean, P., 2013.
963 LAFARA: A new underground laboratory in the French Pyrénées for ultra low-level gamma-ray
964 spectrometry. J. Environ. Radioact. 116, 152–158. https://doi.org/10.1016/j.jenvrad.2012.10.002

965 van Beek, P., Sternberg, E., Reyss, J.L., Souhaut, M., Robin, E., Jeandel, C., 2009. 228Ra/226Ra and
966 226Ra/Ba ratios in the Western Mediterranean Sea: Barite formation and transport in the water
967 column. Geochim. Cosmochim. Acta 73, 4720–4737. https://doi.org/10.1016/j.gca.2009.05.063

968 Woźniak, S.B., Stramski, D., Stramska, M., Reynolds, R.A., Wright, V.M., Miksic, E.Y., Cichocka,
969 M., Cieplak, A.M., 2010. Optical variability of seawater in relation to particle concentration,
970 composition, and size distribution in the nearshore marine environment at Imperial Beach,
971 California. J. Geophys. Res. Ocean. 115, 1–19. https://doi.org/10.1029/2009JC005554

972 Wu, J., Rabouille, C., Charmasson, S., Reyss, J.L., Cagnat, X., 2018. Constraining the origin of
973 recently deposited particles using natural radionuclides 7Be and 234Thex in deltaic sediments.
974 Cont. Shelf Res. 165, 106–119. https://doi.org/10.1016/j.csr.2018.06.010

975 Young, J.A., Silker, W.B., 1980. Aerosol deposition velocities on the Pacific and Atlantic oceans
976 calculated from7Be measurements. Earth Planet. Sci. Lett. 50, 92–104.
977 https://doi.org/10.1016/0012-821X(80)90121-1

978 Zunino, P., Lherminier, P., Mercier, H., Daniault, N., García-Ibáñez, M.I., Pérez, F.F., 2017. The
979 GEOVIDE cruise in May-June 2014 reveals an intense Meridional Overturning Circulation over
980 a cold and fresh subpolar North Atlantic. Biogeosciences 14, 5323–5342.
981 https://doi.org/10.5194/bg-14-5323-2017

982